NACA TN 2365 6978

TECH LIBRARY KAFB, NM
0065627

NATIONAL ADVISORY COMMITTEE FOR AERONAUTICS

TECHNICAL NOTE 2365

ANALYTICAL EVALUATION OF AERODYNAMIC CHARACTERISTICS OF TURBINES WITH NONTWISTED ROTOR BLADES

By William R. Slivka and David H. Silvern

Lewis Flight Propulsion Laboratory
Cleveland, Ohio

Washington
May 1951

AFMDC
TECHNICAL LIBRARY

TECH LIBRARY KAFB, NM
0065627

NATIONAL ADVISORY COMMITTEE FOR AERONAUTICS

TECHNICAL NOTE 2365

ANALYTICAL EVALUATION OF AERODYNAMIC CHARACTERISTICS OF TURBINES WITH NONTWISTED ROTOR BLADES

By William R. Slivka and David H. Silvern

SUMMARY

An analytical investigation was made of the aerodynamic characteristics (relative rotor-entrance Mach number, reaction factor, rotor turning angle, radial variation of specific work output, and rotor-exit tangential-velocity head) of single-stage turbines with nontwisted rotor blades, and an evaluation of these characteristics on the basis of the simplified-radial-equilibrium analysis was made by comparison with the corresponding characteristics of free-vortex turbines. In order to obtain an indication of the effects of the radial shifts of weight flow on the significant parameters discussed in the comparison, further analyses were made of a contemporary single-stage turbine where the forces due to the curvature of the streamlines in the axial-radial plane are approximated.

On the basis of the simplified-radial-equilibrium analysis and the analysis accounting for streamline curvature in the axial-radial plane, the aerodynamic characteristics of nontwisted-rotor-blade turbines are approximately those of free-vortex turbines intended for similar application for values of hub-tip-radius ratios that are used in current turbines.

INTRODUCTION

Nontwisted turbine blades were first used in early steam-turbine practice without regard to radial variations in flow conditions. Although more recently steam-turbine designers have recognized that certain radial variations of flow do exist, consideration of manufacturing costs have generally limited the extent to which these radial variations have been accounted for. For aircraft gas turbines, the great importance of high single-stage power output, together with high turbine efficiency, has required that allowances for radial variations in flow conditions be made in design techniques. These techniques are generally based on either free-vortex flow or constant specific weight flow, either of which results in twisted turbine rotor blades.

Recent research has indicated that it is desirable to incorporate multiple cooling passages within turbine rotor blades (reference 1). The manufacture of such cooled blades will be simplified if the rotor blades can be of uniform camber and without twist along the blade length, that is, nontwisted rotor blades. 2117

The design of nontwisted rotor blades in combination with nontwisted stator blades is discussed in reference 2. Analysis of the data of reference 2 shows that the relative flow angle at the rotor entrance varies along the radius. Variation of the relative rotor-entrance flow angle, combined with nontwisted rotor blades, however, will very likely result in increased losses in a turbine that has high aerodynamic loads and a high relative rotor-entrance Mach number.

In the analysis made at the NACA Lewis laboratory and presented herein, the use of nontwisted rotor blades in combination with twisted stator blades is considered as a method of obtaining structural simplicity and efficient aerodynamic performance of turbines. The manufacture of twisted and cooled stator blades is presumably easier than twisted and cooled rotor blades because of the freedom in selecting materials and manufacturing processes that the low stator-blade stress provides.

A general method of design analysis for various types of radial-flow variation is presented in reference 3 for (a) the simplified-radial-equilibrium case where the forces due to the curvature of the streamlines in a axial-radial plane are neglected, and (b) the radial-equilibrium case where these forces are included. No detailed analysis is made, however, for the particular case of nontwisted-rotor-blade turbines.

The purpose of the present report is to investigate the aerodynamic characteristics of nontwisted-rotor-blade turbines and to evaluate the characteristics of this type of design by comparison with the characteristics of free-vortex designs. The free-vortex turbine was chosen for comparison because it is one of the most common types used in current design practice.

The evaluation is based on the simplified-radial-equilibrium analysis, where the parameters of weight flow, relative rotor-entrance Mach number, reaction factor, rotor turning angle, specific work output, and rotor-exit tangential-velocity head of single-stage nontwisted-rotor-blade turbines are compared with the corresponding parameters of single-stage free-vortex turbines. Further analysis is then made of a particular single-stage turbine where the forces due to the curvature

of the streamlines in the axial-radial plane are approximated in order to obtain an indication of the effects of the radial shifts of weight flow on the parameters investigated in the comparison.

2117

ANALYSIS

The aerodynamic design of a turbine may be divided into two phases. The first is the analysis of the radial variations of the velocity vectors at the stator and rotor exit and the second is the design of the blade profiles to achieve the desired velocity diagrams. The design of the blade profiles and the effect on the conditions of the gas at the rotor entrance and exit are not considered in this analysis. Throughout the analysis, the relative air angles at the rotor entrance and exit are assumed equal to the rotor-blade angles. The symbols used herein are defined in appendix A.

Simplified-Radial-Equilibrium Analysis

Flow at rotor entrance. - An analysis of the flow conditions at the rotor entrance, with the specification that the relative rotor-entrance angle is constant along the radius, is presented in appendix B. In this analysis, the following assumptions were made: axial symmetry, constant total temperature along the radius, constant entropy along the radius, and simplified radial equilibrium. The following equation relating the radius ratio r/r_o to the velocity-vector-diagram terms (fig. 1) is obtained:

$$\frac{r}{r_o} = e^{-\frac{1}{2}\left(\frac{1}{\cos^2\beta + 1}\right)\left\{\log_e\left[\left(\frac{V_u}{U}\right)^2 + \frac{\tan^2\beta}{2}\left(\frac{V_u}{U} - 1\right)^2\right] - \frac{\sin 2\beta}{\sqrt{2}} \arctan\left[\frac{\tan\beta}{\sqrt{2}}\left(1 - \frac{U}{V_u}\right)\right]\right\}} \tag{1}$$

This equation was obtained by integrating equation (B13) between the limits of 1 and V_u/U in the right member and 1 and r/r_o in the left member.

Equation (1) was used in the construction of figure 2, where V_u/U is plotted against r/r_o for constant values of β. Lines of constant stator-exit angle α varying from 10° to 45° are also plotted. The α lines were determined from the expression

$$\tan\alpha = \left(1 - \frac{U}{V_u}\right)\tan\beta \tag{2}$$

Figure 2 was used in the evaluation of the nontwisted-rotor-blade turbines to determine the radial variations of velocity vectors. The chart was used as follows: Values of β_m, $(V_u/U)_m$, and U_m were assigned and the corresponding value of $(r/r_o)_m$ was then determined. Other values of r/r_o were determined from the following expression: 2117

$$\frac{r}{r_o} = \left(\frac{r}{r_o}\right)_m \frac{r}{r_m}$$

For each value of r/r_o, the corresponding values of V_u/U are obtained from the chart for the given value of β. With these parameters known, the velocity-vector diagrams are then calculated and, with given values of stagnation temperature and pressure, the gas properties along the radius may be easily calculated.

In order to determine quickly the aerodynamic characteristics of nontwisted-rotor-blade turbines when a number of possible turbine-design conditions are being investigated, figure 3 was constructed for values of stator-exit angle α from 10° to 45°. A weight-flow parameter $\frac{w\sqrt{T'}}{p\ \pi r_o^2}$ is plotted against radius ratio $\frac{r}{r_o}$ for constant values of β, $\gamma = 1.3$, and values of M_o from 1.0 to 0.5, where M_o is defined as U_o/a_{cr}. Lines of constant relative rotor-entrance Mach number M_w and a line that divides the charts into supersonic and subsonic stator-exit conditions are also plotted. The method of construction of figure 3 is presented in appendix C.

The use of figure 3 in conjunction with the use of figure 2 may be illustrated as follows: For given values of V_u, β, and U at some radius, the corresponding value of r/r_o is obtained from figure 2. With U and r/r_o known, U_o is calculated and, with a given design value of T', M_o is then determined. With p' known and with an assumed value of flow coefficient that accounts for the effects of annulus-wall boundary layer and blade wakes in reducing the flow area, the limits of r/r_o that pass the desired weight flow are obtained from figure 3. At these limits of r/r_o, the relative rotor-entrance Mach number and the stator-exit angle are obtained from figure 3.

The flow conditions for the free-vortex turbines were determined in accordance with the methods presented in reference 3.

Flow at rotor exit. - An analysis of the flow conditions at the rotor exit, with the specification that the relative rotor-exit angle is constant along the radius, is presented in appendix D. In this analysis, the following assumptions were made: axial symmetry, constant entropy along the radius, simplified radial equilibrium, and streamlines at the rotor entrance and exit lying on the same radius. The following equation defining the change of tangential velocity with radius as derived in appendix D applies:

$$\frac{dV_{u,3}}{dr} = \frac{-\frac{V_{u,3}^2}{U} + V_{u,3}\left(1 + \tan^2 \beta_3\right) - r\frac{dV_{u,2}}{dr} - V_{u,2} - U \tan^2 \beta_3}{r\left(\frac{V_{u,3}}{U} - 1\right)\left(1 + \tan^2 \beta_3\right)} \tag{3}$$

The conditions at the rotor exit were determined from equation (3) in the following manner: The value of $V_{u,3}$ was assigned at the mean radius and the value of β_3 necessary to satisfy continuity was determined from figure 4 and the method presented in appendix E. This method determines β_3 from an evaluation of flow conditions at the mean radius by the assumption that the specific weight flow at the mean radius is equal to the average specific weight flow. When the values of $V_{u,3,m}$, β_3, and rotor-entrance conditions are known, a solution of equation (3) was obtained by using the Runge-Kutta method of numerical integration, as presented in reference 4. With this information, the specific weight flow was then integrated to determine the accuracy of the value of β_3 obtained from figure 4. In all cases considered, this first approximation was sufficiently accurate. It should be noted that, because of the small values of exit tangential velocity existing in most cases, the use of large increments of radius yielded sufficiently accurate results in the numerical integration.

The flow conditions for the free-vortex turbines were determined in accordance with the methods presented in reference 3.

Radial Equilibrium Accounting for Streamline Curvature

In reference 3, it is shown that the assumption of simplified radial equilibrium leads to errors in the determination of the radial variations of flow. This result especially applies to nontwisted-rotor-blade turbines where large radial shifts of weight flow occur. This section will be devoted to a method of approximating the forces

due to the curvature of the streamlines in the axial-radial plane in order to obtain an indication of the effects of the radial shifts of weight flow on the results obtained by the simplified-radial-equilibrium analysis.

Flow at rotor entrance. - The equations describing the radial variation of velocity at the rotor entrance midway between the stator and rotor blades for nontwisted-rotor-blade turbines and free-vortex turbines that include the additional force term due to the curvature of the streamlines in the axial-radial plane are presented in appendix F. The assumptions used in this analysis were: axial symmetry, constant total temperature along the radius, and constant entropy along the radius. The equations that define the variation of the axial velocity with radius for the cases considered are as follows: 2117

Nontwisted rotor blade:

$$\frac{d\left(\frac{V_x}{U}\right)}{d\left(\frac{r}{r_m}\right)} = -\frac{1}{\frac{r}{r_m}} \frac{2 + 4\left(\frac{V_x}{U}\right)\cot\beta + \left(\frac{V_x}{U}\right)^2\left[-\frac{r_m}{C}\left(\frac{r}{r_m}\right) + \left(1 + 2\cot^2\beta\right)\right]}{\frac{V_x}{U}\csc^2\beta + \cot\beta} \tag{4}$$

Free-vortex rotor blade:

$$\frac{dV_x}{dr} = \frac{V_x}{C} \tag{5}$$

where C is the radius of curvature of the streamline in the axial-radial plane at the entrance station (fig. 1). It was found to be more convenient to present these equations in terms of the radial variation of axial velocity instead of the radial variation of tangential velocity.

A simplified method for the solution of these equations for a multistage machine is presented in reference 3 with the assumption that the form of the streamlines in the axial-radial plane is sinusoidual. For a single-stage machine, it is possible that the streamlines will be more closely approximated by the equation

$$r = r_{x=\infty} + \Delta e^{-\frac{1}{2}\left(\frac{x}{b}\right)^2}$$

because this equation will satisfy the condition of the streamlines lying on the same radius at $\pm\infty$ and having a maximum deflection between the blade rows.

2117

It is assumed in this analysis that the maximum deflection of the streamlines occurs midway between the stator and the rotor inasmuch as it is probable that at this station the specific weight flow has its greatest variation. It is further assumed that the inflection point of the streamlines occurs at the midchord point of the stator (fig. 1).

When these assumptions are used, the curvature of the streamlines at the point of the streamlines midway between the stator and rotor blades equals $-\Delta/b^2$, where Δ is the maximum deflection $(r_{max} - r)$ and b is the axial distance from the point of inflection to the point of maximum deflection. The following equations, which were solved by the numerical methods previously used, were obtained by substituting for the radius of curvature in equations (4) and (5):

Nontwisted rotor blades:

$$\frac{d\left(\frac{V_x}{U}\right)}{d\left(\frac{r}{r_m}\right)} = -\frac{1}{\frac{r}{r_m}} \frac{2 + 4\left(\frac{V_x}{U}\right)\cot\beta + \left(\frac{V_x}{U}\right)^2\left[\left(\frac{r_m\Delta}{b^2}\right)\left(\frac{r}{r_m}\right) + (1 + 2\cot^2\beta)\right]}{\frac{V_x}{U}\csc^2\beta + \cot\beta} \tag{6}$$

Free-vortex rotor blades:

$$\frac{dV_x}{dr} = \frac{-V_x\Delta}{b^2} \tag{7}$$

Inasmuch as Δ is not directly determinable, a trial solution is necessary. The first approximation is found by integrating equations (6) and (7) with Δ equal to zero (simplified-radial-equilibrium case). From the velocities and the densities so determined, the weight flow was plotted as a function of radius. The radii that divide the weight flow into equal parts were determined and the deviation of these radii from those determined by dividing the annulus area in equal parts (constant specific weight flow at rotor entrance) were found. These deviations Δ were then used to calculate a second approximation. This procedure was repeated until the assumed values of Δ checked the final calculated values. After continuity was satisfied, the value of $V_{x,m}$ did not change with successive approximations of Δ.

Flow at rotor exit. - At the rotor exit, it was assumed that the effect of the curvature of the streamlines in the axial-radial plane is negligible. The analysis as presented in appendix D is therefore applicable. However, U_2 is not assumed equal to U_3 as in the simplified-radial-equilibrium analysis and equation (D6) was therefore used, rather than equation (3). The conditions at the rotor exit were determined from equation (D6) by the same method of solution as was previously presented in the section on the flow at the rotor exit for the simplified-radial-equilibrium analysis.

COMPARISON OF RESULTS

Simplified-Radial-Equilibrium Analysis

The aerodynamic characteristics of weight flow, relative rotor-entrance Mach number, reaction factor, rotor turning angle, work output, and specific rotor-exit tangential-velocity head were determined for nontwisted-rotor-blade and free-vortex turbines with the following operating conditions; these conditions were chosen to cover the range of current design limitations:

Case	Stagnation inlet temperature, T'_1 ($^{\circ}R$)	Mean-radius stagnation-pressure ratio, $(p_1'/p_3')_m$	Mean-radius blade speed, U_m (ft/sec)	Mean-radius rotor-exit tangential velocity, $(V_{u,3})_m$ (ft/sec)	Mean-radius relative rotor-entrance angle, β_m (deg)	Turbine internal efficiency, η_T
1	2500	1.5	900	0	40, 50, 60	0.85
2	2500	2.0	1100	0	40, 50, 60	.85
3	2500	2.5	1300	0	40, 50, 60	.85
4	2500	3.0	1400	0	40, 50, 60	.85
5	2500	2.5	1300	$-0.2\ U_m$	40, 50, 60	.85

A weight-flow ratio $\overline{w}$ defined as

$$\overline{w} = \frac{2\pi \int_{r_h}^{r_t} \rho V_x\, r \cdot dr}{(\rho V_x)_m\, \pi(r_t^2 - r_h^2)}$$

2117

is plotted in figure 5 against hub-tip-radius ratio for the preceding cases. The significance of the weight-flow ratio is two-fold: (1) It demonstrates the deviation of the actual weight flow as compared with the weight flow determined from the mean-radius condition; and (2) it serves to demonstrate the comparison of the actual weight flow of a nontwisted-rotor-blade and a free-vortex turbine, with both turbines having the same mean-radius conditions. For all cases considered, $\overline{w} = 1$ for the free-vortex turbines. For the nontwisted-rotor-blade turbines, however, $\overline{w} < 1$. This weight-flow ratio decreased as the hub-tip-radius ratio decreased, giving a minimum value for the cases considered of approximately 0.89 at a hub-tip-radius ratio of 0.6 for case 5. At a hub-tip-radius ratio of 0.75, a value that more closely approximates the values used in current turbines, the minimum value of the weight-flow ratio was approximately 0.96.

In order to make the comparison of the aerodynamic characteristics of the nontwisted-rotor-blade and free-vortex turbines valid for equal weight flow for the same hub-tip-radius ratio and mean radius, the axial velocity of the free-vortex turbines was decreased so that the weight flow of the two types of turbine were equal for every hub-tip-radius ratio. This equality resulted in a change in the relative rotor-entrance angle at the mean radius for the free-vortex turbine at every hub-tip-radius ratio and the remainder of the comparison is made on this basis. These results are presented in figures 6 to 11, where the parameters of relative rotor-entrance Mach number, reaction factor, radial variation of work output, rotor turning angle, and specific rotor-exit tangential-velocity head are plotted for both the nontwisted-rotor-blade and free-vortex turbines. Inasmuch as the magnitude of the values of these parameters for cases 2 and 3 were within the limits of the values of the parameters for cases 1 and 4, cases 2 and 3 are omitted for the remainder of the comparison.

Relative rotor-entrance Mach number. - The value of the maximum allowable relative rotor-entrance Mach number is one of the limiting factors in the design of turbines. Because the maximum value of this Mach number always occurs at the hub of the machine, the comparison of Mach number for the nontwisted-rotor-blade and the free-vortex turbines was restricted to comparison at the hub. The relative rotor-entrance Mach number at the hub is plotted in figure 6 against hub-tip-radius ratio for the cases considered. For all the cases considered, the Mach number for the nontwisted-rotor-blade turbines was greater than the Mach number for the free-vortex turbines. At a hub-tip-radius ratio of 0.6, the Mach number for the nontwisted-rotor-blade turbines was approximately 0.02 to 0.16 greater than the Mach

number for the free-vortex turbines; the higher values occur at the higher turbine pressure ratios and higher relative rotor-entrance angles. The magnitude of the effect on turbine losses associated with increases of Mach number of the order discussed is unknown and will depend on the blade loading and the critical inlet Mach number of the particular blade sections.

Reaction factor. - The reaction factor ψ defined by $\psi = (W_3^2-W_2^2)/W_2^2$ is a measure of the static-pressure change across the rotor. The value of ψ based on isentropic flow is equal to zero for impulse blading and this value is often considered a limiting point in contemporary turbine design. In general, the values of ψ decrease from tip to hub, which makes the hub of the machine critical with regard to ψ. The comparison of the reaction factor was therefore restricted to the hub of the machine. A plot of hub reaction factor ψ_h against hub-tip-radius ratio is shown in figure 7 for the nontwisted-rotor-blade and the free-vortex turbines. For cases 1 and 4, the reaction factors for both types of turbine are approximately equal for all hub-tip-radius ratios and relative rotor-entrance angles. For case 5, the reaction factor for the free-vortex turbines is from 0 to approximately 0.2 greater than the reaction factor for the nontwisted-rotor-blade turbines. The magnitude of these differences is considered negligible.

Work output. - Two problems are associated with radial variations of specific work output: (1) the problem of possible losses associated with the mixing to constant conditions and the possible induced losses arising from secondary flows associated with radial gradients of work output, and (2) the problem of obtaining a given average specific work output. The specific work output for the nontwisted-rotor-blade turbines varies along the radius, whereas the specific work output is constant along the radius for the free-vortex turbines, as shown in figure 8, where a ratio of specific work to specific work at the mean radius is plotted against radius ratio r/r_m for the cases considered. Cases 1, 4, and 5 show similar variations. For hub-tip-radius ratios of 0.6, this variation from the value at the mean radius was of the order of 5, 10, and 15 percent for relative rotor-entrance angles of 40°, 50°, and 60°, respectively. For hub-tip-radius ratios of 0.75, which more closely approximate the values used in current turbines, this variation is of the order of 2.5, 5, and 7.5 percent for relative rotor-entrance angles of 40°, 50°, and 60°, respectively.

2117

It is estimated that the mixing losses associated with the variation of specific work output presented are negligible, which is based on the assumption that only that part of the velocity head that remains after the flow is mixed to constant conditions is considered recoverable. The induced secondary losses are also estimated to be small.

In order to determine the effect of the variation of specific work output on the over-all work output, an average-specific-work ratio $\bar{h}$ defined as

$$\bar{h} = \frac{\int_{r_h}^{r_t} U(V_{u,2}-V_{u,3})\rho V_x r \, dr}{\int_{r_h}^{r_t} \left[U(V_{u,2}-V_{u,3})\right]_m \rho V_x r \, dr}$$

is plotted in figure 9 against hub-tip-radius ratio for the nontwisted-rotor-blade and the free-vortex turbines. It may be seen from figure 9 that, if the nontwisted-rotor-blade turbine is designed for a specific work output at the mean radius, the average work output will be a maximum of approximately 2 percent less than the value based on the mean radius.

Rotor turning angle. - Another factor in turbine design is the rotor-blade turning angle. In free-vortex turbines, the turning angle is maximum at the hub where the relative rotor-entrance Mach numbers and the reaction factor are most critical. The rotor-blade-hub turning angle is plotted against hub-tip-radius ratio for the nontwisted-rotor-blade and the free-vortex turbines in figure 10. In every case, the turning angle, and thus the blade loading, for the nontwisted-rotor-blade turbine was less than the turning angle for the free-vortex turbine, so that it is probable that the use of higher relative rotor-hub-entrance Mach numbers and lower reaction factors is possible with nontwisted-rotor-blade turbines than with corresponding free-vortex turbines.

Rotor-exit tangential-velocity head. - For nontwisted-rotor-blade turbines, it is impossible to obtain zero values of exit tangential velocity at all radii. The average specific rotor-exit tangential-velocity head (that is, the mass-averaged value of $V_{u,3}^2/2gJ$) is plotted against hub-tip-radius ratio in figure 11 for the cases considered. Charging this velocity head as a loss to the turbine is equivalent to a maximum decrease of efficiency of the nontwisted-rotor-blade turbine of approximately 1 percent compared with the free-vortex turbines.

Radial Equilibrium Accounting for Streamline Curvature

In order to obtain an indication of the effects of the radial shifts of weight flow on the design parameters, as discussed in the preceding section, the analysis accounting for streamline curvature in the axial-radial plane was applied to a nontwisted-rotor-blade and a free-vortex turbine. The following design conditions chosen were those of a typical contemporary turbine: 2117

Total-pressure ratio	2.28
Turbine-inlet temperature, °R	2000
Turbine internal efficiency	0.85
Weight flow, lb/sec	75.5
Turbine speed, rpm	11,500
Tip radius, in.	13.0
Hub radius, in.	9.0
Hub-tip-radius ratio	0.693
Stator aspect ratio (based on axial chord)	2.0
Rotor aspect ratio (based on axial chord)	1.78
Axial clearance between stator and rotor, in.	0.72

The results of this analysis are presented in figures 12 to 15, together with the results of a simplified-radial-equilibrium analysis based on the same design conditions. The amount of radial shift encountered in the axial clearance space midway between the rotor and the stator is plotted against radius ratio r/r_m in figure 12. It may be seen that the deviation of the streamlines is toward the tip for the free-vortex turbine and is toward the hub for the nontwisted-rotor-blade turbine. In both cases the deviations are larger for the simplified-radial-equilibrium analysis. In the free-vortex turbines, however, the radial shift of flow is smaller than in the nontwisted-rotor-blade turbines, especially in the case where the curvature of the streamlines is considered. The stator-exit-angle variation for the nontwisted-rotor-blade turbine is presented in figure 13 for both the simplified-radial-equilibrium analysis and the analysis accounting for streamline curvature. It may be seen that the variation in stator-exit angle is less than 1°. A radial variation of circulation across the stator exists with this type of stator. The effect of this variation of circulation on turbine performance is unknown. It is noted, however, that the radial gradient of circulation was less than the circulation gradient of a wheel-type stator where $V_u = Kr$ for the same mean-radius conditions and the wheel-type stator has been used in current compressor designs with no decrease in efficiency.

Relative rotor-entrance Mach number. - In the discussion of relative rotor-entrance Mach number for the simplified-radial-equilibrium analysis, it was found that the relative Mach number at the hub was

slightly higher for the nontwisted-rotor-blade turbine than for the free-vortex turbine. This difference was also found for the typical turbine design shown in figure 14, where the relative rotor-entrance Mach number is plotted against radius ratio r/r_m for the simplified-radial-equilibrium analysis and for the analysis accounting for streamline curvature. On the basis of the analysis accounting for the curvature of the streamlines, however, the radial pressure variation has changed so that the velocities at the hub for the free-vortex turbine increased and the velocities at the hub for the nontwisted-rotor-blade turbine decreased. The result was an increase in Mach number at the hub of 0.05 for the free-vortex turbine and a decrease of 0.08 for the nontwisted-rotor-blade turbine. Thus, the comparison of relative rotor-entrance Mach number based on the simplified-radial-equilibrium analysis may be considered conservative.

Reaction factor. - The effect of streamline curvature on the reaction factor based on a simplified-radial-equilibrium analysis is presented in figure 15, where the reaction factor ψ is plotted against radius ratio r/r_m. On the basis of the analysis accounting for the streamline curvature, the reaction factor at the hub of the turbine decreased from -0.21 to -0.26 for the free-vortex turbine and increased from -0.11 to 0.03 for the nontwisted-rotor-blade turbine. It may be concluded that the comparison of reaction factor may also be considered conservative.

The other design parameters of rotor turning angle, specific work output, and rotor-exit tangential velocity were also investigated and it was found that the variation from the results of the simplified-radial-equilibrium analysis due to streamline curvature was negligible.

CONCLUSION

A comparison of the turbine aerodynamic characteristics (relative rotor-entrance Mach number, reaction factor, rotor turning angle, radial variation of specific work output, and specific rotor-exit tangential-velocity head) was made on the basis of the simplified-radial-equilibrium analysis for nontwisted-rotor-blade and free-vortex turbines. Further analysis was made of a typical contemporary turbine approximating the forces due to the curvature of the streamlines in an axial-radial plane to obtain an indication of the effects of the radial shifts of weight flow on the results obtained by the simplified-radial-equilibrium analysis.

It was found that the aerodynamic characteristics of nontwisted-rotor-blade turbine are approximately those of a free-vortex turbine designed for similar service for values of hub-tip-radius ratios that are used in current turbines.

2117

Lewis Flight Propulsion Laboratory,
National Advisory Committee for Aeronautics,
Cleveland, Ohio, January 4, 1951.

APPENDIX A

SYMBOLS

The following symbols are used in this report:

A	annulus area, sq ft
a_{cr}	velocity of sound, based on critical temperature, ft/sec
b	axial distance from point of inflection to point of maximum deflection of streamlines, ft
C	radius of curvature of streamline in axial-radial plane, ft
c_p	specific heat, ft-lb/(lb)($^{\circ}$R)
g	acceleration due to gravity, ft/sec^2
h	specific enthalpy, ft/lb
$\overline{h}$	specific-work ratio
J	mechanical equivalent of heat, ft-lb/Btu
K	function of (g, c_p, and γ)
M	Mach number
p	absolute pressure, lb/sq ft
R	gas constant, ft-lb/($^{\circ}$R)(lb)
r	radius, ft
T	absolute temperature, $^{\circ}$R
U	blade velocity, ft/sec
V	absolute gas velocity, ft/sec
W	relative gas velocity, ft/sec
w	gas weight flow, lb/sec
$\overline{w}$	gas-weight-flow ratio

x axial distance, ft

α angle of absolute velocity with tangential direction, deg

β angle of relative velocity with tangential direction, deg

γ ratio of specific heats

Δ maximum deflection of streamlines in radial direction, ft

η_T turbine efficiency based on stagnation conditions

ρ density, lb/cu ft

φ angle between streamline and axial direction, deg

ψ reaction factor

ω angular velocity, radians/sec

Subscripts:

o reference radius

1 stator entrance

2 stator exit, rotor entrance

3 rotor exit

h turbine hub

m mean radius

r radial

t turbine tip

u tangential

w relative

x axial

Superscript:

' stagnation state

2117

2117

APPENDIX B

RADIAL VARIATION OF VELOCITY AT ROTOR ENTRANCE FOR SIMPLIFIED-RADIAL-EQUILIBRIUM ANALYSIS

The following analysis of the flow conditions at the rotor entrance is made with the specification that the relative rotor-entrance angle is constant along the radius. It will be assumed that simplified radial equilibrium exists in the axial-radial plane; that is, the forces due to the curvature of the streamlines are zero. Axial symmetry, constant total temperature along the radius, and constant entropy along the radius will also be assumed.

From vector-diagram considerations (fig. 1),

$$\tan \beta = \frac{V_x}{(V_u - U)} = \frac{V_x}{(V_u - \omega r)} \tag{B1}$$

and differentiation of equation (B1) with respect to the radius gives

$$\frac{dV_x}{dr} = \tan \beta \left(\frac{dV_u}{dr} - \omega\right) \tag{B2}$$

The energy equation for adiabatic compressible flow may be written as

$$\frac{V_u^{\,2}}{2g} + \frac{V_x^{\,2}}{2g} + h = h' \tag{B3}$$

and differentiation of equation (B3) with respect to the radius, with $dh'/dr = 0$, gives

$$\frac{V_u}{g}\frac{dV_u}{dr} + \frac{V_x}{g}\frac{dV_x}{dr} + \frac{dh}{dr} = 0 \tag{B4}$$

For simplified radial equilibrium,

$$\frac{V_u^{\,2}}{gr} = \frac{dp}{\rho\, dr} \tag{B5}$$

With constant entropy along the radius,

$$\frac{dh}{dr} = \frac{dp}{\rho\, dr} \tag{B6}$$

Equations (B1), (B2), and (B4) combine to yield

$$\frac{V_u}{g}\frac{dV_u}{dr} + \frac{\tan^2\beta}{g}(V_u-\omega r)\left(\frac{dV_u}{dr} - \omega\right) + \frac{dh}{dr} = 0 \tag{B7}$$

2117

and equations (B5) and (B6) combine to yield

$$\frac{dh}{dr} = \frac{V_u^2}{gr} \tag{B8}$$

The substitution of V_u^2/gr for dh/dr in equation (B7) yields

$$\frac{V_u}{g}\frac{dV_u}{dr} + \frac{\tan\beta}{g}(V_u-\omega r)\tan\beta\left(\frac{dV_u}{dr} - \omega\right) + \frac{V_u^2}{gr} = 0 \tag{B9}$$

Simplifying equation (B9) and making the substitution for $\omega r = U$ yields

$$\frac{dV_u}{dr} = -\frac{V_u}{r}\frac{V_u - U\tan^2\beta + \frac{U^2}{V_u}\tan^2\beta}{V_u - U\tan^2\beta + V_u\tan^2\beta} \tag{B10}$$

When the numerator and the denominator of the right side are divided by V_u, equation (B10) may be written as

$$\frac{dV_u}{dr} = -\frac{V_u}{r}\frac{1 - \frac{U}{V_u}\tan^2\beta + \frac{U^2}{V_u^2}\tan^2\beta}{1 - \frac{U}{V_u}\tan^2\beta + \tan^2\beta} \tag{B11}$$

Differentiating V_u/U with respect to r yields

$$\frac{d\left(\frac{V_u}{U}\right)}{dr} = -\frac{1}{r^2}\frac{V_u}{\omega} + \frac{1}{U}\frac{dV_u}{dr} \tag{B12}$$

Substituting equation (B11) for dV_u/dr in equation (B12) and dividing the numerator and the denominator by r_o yields:

$$\frac{d\left(\frac{r}{r_o}\right)}{\frac{r}{r_o}} = \frac{-d\left(\frac{V_u}{U}\right)}{\frac{V_u}{U}\left(1 + \frac{1 - \frac{U}{V_u}\tan^2\beta + \frac{U^2}{V_u^2}\tan^2\beta}{1 - \frac{U}{V_u}\tan^2\beta + \tan^2\beta}\right)} \tag{B13}$$

The limits will be assigned as $V_u/U = 1$ to V_u/U and $r/r_o = 1$ to r/r_o.

Integrating equation (B13) results in

$$\frac{r}{r_o} = e^{-\frac{1}{2}\left(\frac{1 + \tan^2\beta}{2 + \tan^2\beta}\right)} \left\{ \log_e\left[\left(\frac{V_u}{U}\right)^2 - 2\left(\frac{V_u}{U}\right)\left(\frac{\tan^2\beta}{2 + \tan^2\beta}\right) + \frac{\tan^2\beta}{2 + \tan^2\beta}\right] + \right.$$

$$\left. \frac{2\left(\frac{\tan^2\beta}{2 + \tan^2\beta} - \frac{\tan^2\beta}{1 + \tan^2\beta}\right)}{\sqrt{\frac{\tan^2\beta}{2 + \tan^2\beta}\left(1 - \frac{\tan^2\beta}{2 + \tan^2\beta}\right)}} \text{arc tan} \frac{\frac{V_u}{U} - \frac{\tan^2\beta}{2 + \tan^2\beta}}{\sqrt{\frac{\tan^2\beta}{2 + \tan^2\beta}\left(1 - \frac{\tan^2\beta}{2 + \tan^2\beta}\right)}} \right\} \Bigg|_1^{\frac{V_u}{U}} \tag{B14}$$

Substituting the limits in the right member results in

$$\frac{r}{r_o} = e^{-\frac{1}{2}\left(\frac{1}{\cos^2\beta + 1}\right)} \left\{ \log_e\left[\left(\frac{V_u}{U}\right)^2 + \frac{\tan^2\beta}{2}\left(\frac{V_u}{U} - 1\right)^2\right] - \right.$$

$$\left. \frac{\sin 2\beta}{\sqrt{2}} \text{arc tan}\left[\frac{\tan\beta}{\sqrt{2}}\left(1 - \frac{U}{V_u}\right)\right] \right\} \tag{1}$$

2117

APPENDIX C

CONSTRUCTION OF FIGURE 3 (ROTOR ENTRANCE)

The chart of figure 3 was constructed as follows: An increment of weight flow through an increment of annular area may be expressed as

$$dw = \rho V_x 2\pi r \, dr \tag{C1}$$

The ratio of static to total density may be expressed in terms of the critical velocity as

$$\frac{\rho}{\rho'} = \left[1 - \frac{\gamma-1}{\gamma+1}\left(\frac{V}{a_{cr}}\right)^2\right]^{\frac{1}{\gamma-1}} \tag{C2}$$

Substituting for ρ in equation (C1) yields

$$dw = \rho' \left[1 - \frac{\gamma-1}{\gamma+1}\left(\frac{V}{a_{cr}}\right)^2\right]^{\frac{1}{\gamma-1}} V_x 2\pi r \, dr \tag{C3}$$

Inasmuch as

$$a_{cr}^2 = \frac{2(\gamma-1)}{\gamma+1} g c_p T'$$

$$V_x = (V_u - U) \tan \beta$$

and

$$V^2 = V_u^2 + (V_u - U)^2 \tan^2 \beta$$

equation (C3) may be written as

$$dw = \rho' \left[1 - \frac{V_u^2 + (V_u - U)^2 \tan^2 \beta}{2 g c_p T'}\right]^{\frac{1}{\gamma-1}} (V_u - U) \tan \beta 2\pi r \, dr \tag{C4}$$

Substituting ωr for U in equation (C4), dividing by r_o^2, and making the substitution $\rho' = p'/RT'$, where R is the universal gas constant, yields

$$\frac{RT'dw}{p'\pi r_o^2} = \left\{1 - \frac{\left[\left(\frac{V_u}{U}\right)^2 + \left(\frac{V_u}{U} - 1\right)^2 \tan^2 \beta\right]\left(\frac{r}{r_o}\right)^2 (\omega r_o)^2}{2gc_pT'}\right\}^{\frac{1}{\gamma-1}}$$

$$2\left(\frac{V_u}{U} - 1\right) \omega r_o\left(\frac{r}{r_o}\right)^2 \tan \beta \; d\left(\frac{r}{r_o}\right) \tag{C5}$$

Letting

$$M_o^2 = \frac{(\omega r_o)^2}{2gc_p \frac{\gamma-1}{\gamma+1} T'}$$

$$K = 2gc_p \frac{\gamma-1}{\gamma+1}$$

and dividing equation (C5) by $R\sqrt{T'}$ results in the following expression for the weight-flow parameter:

$$\frac{dw\sqrt{T'}}{p'\pi r_o^2} = \left\{1 - \left[\left(\frac{V_u}{U}\right)^2 + \left(\frac{V_u}{U} - 1\right)^2 \tan^2 \beta\right]\right.$$

$$\left.\frac{\gamma-1}{\gamma+1}\left(\frac{r}{r_o}\right)^2 M_o^2\right\}^{\frac{1}{\gamma-1}} 2\frac{\sqrt{K}}{R}\left(\frac{V_u}{U} - 1\right)\left(\frac{r}{r_o}\right)^2 M_o \tan \beta \; d\left(\frac{r}{r_o}\right) \tag{C6}$$

For given values of M_o, r/r_o was assigned within the range given in figure 2 and values of V_u/U were determined for constant values of β from figure 2. The equation was then numerically integrated within the limits of $r/r_o = 1$ to r/r_o. The results of the integration are presented in figure 3, where $\frac{w\sqrt{T'}}{p'\pi r_o^2}$ is plotted as a function of radius ratio r/r_o for constant values of β for $\gamma = 1.3$. 2117

The lines of constant relative-rotor entrance Mach number and stator-exit angle are plotted on these figures and were determined as follows:

The relative rotor-entrance Mach number may be expressed as

$$M_w = \frac{W}{\sqrt{\gamma g R T}} \tag{C7}$$

From the vector-diagram considerations,

$$W^2 = W_u^2 + V_x^2 = W_u^2 + \tan^2 \beta \, W_u^2$$

then

$$W^2 = (V_u - U)^2 \, (1 + \tan^2 \beta) \tag{C8}$$

and from the definition of total temperature, T may be expressed as

$$T = T' - \frac{\gamma-1}{2\gamma g R} (V_x^2 + V_u^2) \tag{C9}$$

Inasmuch as $V_x^2 = \tan^2 \beta \, (V_u - U)^2$, equation (C9) may be written as

$$T = T' - \frac{\gamma-1}{2\gamma g R} \left[(V_u - U)^2 \tan^2 \beta + V_u^2 \right] \tag{C10}$$

When equations (C8) and (C10) are substituted in equation (C7) squared, the following expression is obtained for M_w^2:

$$M_w^2 = \frac{(V_u-U)^2 \left(1 + \tan^2 \beta\right)}{\gamma g R T' - \frac{\gamma-1}{2}\left[\tan^2 \beta \left(V_u-U\right)^2 + V_u^2\right]} \tag{C11}$$

Dividing the numerator and the denominator of the right member by U^2 and making the substitution of $U^2 = \left(\frac{r}{r_o}\right)^2 U_o^2$ and the substitution of the definition of M_o^2 yield

$$M_w^2 = \frac{\left(\frac{V_u}{U} - 1\right)^2 \left(1 + \tan^2 \beta\right)}{\frac{\gamma+1}{2}\left(\frac{r_o}{r}\right)^2 \frac{1}{M_o^2} - \frac{\gamma-1}{2}\left[\tan^2 \beta\left(\frac{V_u}{U} - 1\right)^2 + \left(\frac{V_u}{U}\right)^2\right]} \tag{C12}$$

From values of V_u/U determined from figure 2 for assigned values of r/r_o and β, M_w was calculated from equation (C12). When M_w was plotted against r/r_o for constant values of β and M_o, lines of constant relative rotor-entrance Mach number were obtained, as presented in figure 3.

The variation of stator-exit angle with radius ratio r/r_o was determined as follows:

From vector-diagram considerations,

$$\tan \alpha = \frac{V_x}{V_u} = \left(1 - \frac{U}{V_u}\right) \tan \beta$$

or

$$\frac{V_u}{U} = \frac{1}{1 - \frac{\tan \alpha}{\tan \beta}} \tag{C13}$$

When constant values of α and β were assigned within the range used in figure 3, V_u/U was calculated using equation (C13). The corresponding value of r/r_o was determined from figure 2 and lines of constant stator-exit angle were plotted against r/r_o in figure 3.

2117

APPENDIX D

RADIAL VARIATION OF TANGENTIAL VELOCITY AT ROTOR EXIT FOR SIMPLIFIED-RADIAL-EQUILIBRIUM ANALYSIS

For the analysis at the rotor exit, as in the analysis at the rotor inlet, it is assumed that simplified radial equilibrium exists in the axial-radial plane; that is, equation (B5) applies.

The energy equation for adiabatic flow along a streamline between the rotor entrance and exit may be written as

$$h_3 + \frac{V_{u,3}^2}{2g} + \frac{V_{x,3}^2}{2g} = h'_2 - \text{work} \tag{D1}$$

Work may be expressed as

$$\frac{V_{u,2}\ U_2}{g} - \frac{V_{u,3}\ U_3}{g} \tag{D2}$$

Inserting the expression given for work into equation (D1) and then differentiating with respect to r yield the following equation:

$$\frac{dh_3}{dr} + \frac{V_{u,3}}{g}\frac{dV_{u,3}}{dr} + \frac{V_{x,3}}{g}\frac{dV_{x,3}}{dr}$$

$$= \frac{dh'_2}{dr} - \frac{U_2}{g}\frac{dV_{u,2}}{dr} + \frac{U_3}{g}\frac{dV_{u,3}}{dr} - \frac{V_{u,2}}{g}\frac{dU_2}{dr} + \frac{V_{u,3}}{g}\frac{dU_3}{dr} \tag{D3}$$

Constant entropy along the radius is again assumed; therefore, as in appendix B,

$$\frac{dh_3}{dr} = \frac{V_{u,3}^2}{gr}$$

2117

Inasmuch as

$$V_{x,3} = \tan \beta_3 \left(V_{u,3}-U_3\right)$$

and

$$\frac{dV_{x,3}}{dr} = \tan \beta_3 \left(\frac{dV_{u,3}}{dr} - \frac{dU_3}{dr}\right)$$

equation (D3) may be written as

$$\frac{V_{u,3}^{\ 2}}{gr} + \frac{V_{u,3}}{g}\frac{dV_{u,3}}{dr} + \frac{\tan^2 \beta_3}{g}\left(V_{u,3}\frac{dV_{u,3}}{dr} - U_3\frac{dV_{u,3}}{dr} - V_{u,3}\frac{dU_3}{dr} + U_3\frac{dU_3}{dr}\right)$$

$$= \frac{dh'_2}{dr} - \frac{U_2}{g}\frac{dV_{u,2}}{dr} + \frac{U_3}{g}\frac{dV_{u,3}}{dr} - \frac{V_{u,2}}{g}\frac{dU_2}{dr} + \frac{V_{u,3}}{g}\frac{dU_3}{dr} \tag{D4}$$

Because $\frac{dh'_2}{dr} = 0$, solving for $\frac{dV_{u,3}}{dr}$ in equation (D4) yields

$$\frac{dV_{u,3}}{dr} = \frac{-\frac{V_{u,3}^{\ 2}}{r} + V_{u,3}\frac{dU_3}{dr} + \tan^2 \beta_3 V_{u,3}\frac{dU_3}{dr} - U_2\frac{dV_{u,2}}{dr} - V_{u,2}\frac{dU_2}{dr} - \tan^2 \beta_3 U_3\frac{dU_3}{dr}}{V_{u,3} + V_{u,3}\tan^2 \beta_3 - U_3 \tan^2 \beta_3 - U_3} \tag{D5}$$

When terms are combined, equation (D5) may be written as

$$\frac{dV_{u,3}}{dr} = \frac{-\frac{V_{u,3}^{\ 2}}{r} + \left[V_{u,3} + \tan^2 \beta_3 \left(V_{u,3}-U_3\right)\right]\frac{dU_3}{dr} - U_2\frac{dV_{u,2}}{dr} - V_{u,2}\frac{dU_2}{dr}}{\left(V_{u,3}-U_3\right)\left(1 + \tan^2 \beta_3\right)} \tag{D6}$$

When it is assumed that $U_2 = U_3$, dividing the numerator and the denominator of the right member by ω results in

$$\frac{dV_{u,3}}{dr} = \frac{-\frac{V_{u,3}^2}{U} + V_{u,3}\left(1 + \tan^2 \beta_3\right) - r\frac{dV_{u,2}}{dr} - V_{u,2} - U \tan^2 \beta_3}{r\left(\frac{V_{u,3}}{U} - 1\right)\left(1 + \tan^2 \beta_3\right)} \tag{3}$$

2117

APPENDIX E

CONSTRUCTION AND USE OF FIGURE 4 FOR DETERMINATION OF ROTOR-EXIT ANGLE

The chart of figure 4 for determining the rotor-exit angle was constructed as follows: From the energy equation

$$\frac{\rho}{\rho'} = \left[1 - \frac{\gamma-1}{\gamma+1}\left(\frac{V}{a_{cr}}\right)^2\right]^{\frac{1}{\gamma-1}}$$

where

$$a_{cr} = \sqrt{\frac{2}{\gamma+1}\gamma g R T'}$$

and from the exit-velocity vector diagram

$$\left(\frac{V}{a_{cr}}\right)^2 = \left(\frac{V_x}{a_{cr}}\right)^2 + \left(\frac{V_u}{a_{cr}}\right)^2$$

the following expression is derived:

$$\frac{\rho V_x}{\rho' a_{cr}} = \left[1 - \frac{\gamma-1}{\gamma+1}\left(\frac{V_x^2 + V_u^2}{a_{cr}^2}\right)\right]^{\frac{1}{\gamma-1}} \frac{V_x}{a_{cr}} \tag{E1}$$

For given values of $\frac{V_u}{a_{cr}}$ ranging from 0 to 1.2 and values of $\frac{V_x}{a_{cr}}$ ranging from 0 to 1.0, the absolute velocity ratio $\frac{V}{a_{cr}}$ and corrected weight-flow parameter $\frac{\rho V_x}{\rho' a_{cr}}$ were calculated for $\gamma = 1.30$. The

results are presented in figure 4, where $\frac{V}{a_{cr}}$ is plotted against $\frac{\rho V_x}{\rho' a_{cr}}$ with lines of constant values of $\frac{V_x}{a_{cr}}$ and $\frac{V_u}{a_{cr}}$ Superimposed are lines of constant absolute flow angles, which were determined from the following expression:

2117

$$\tan^{-1} \alpha = \frac{V_x/a_{cr}}{V_u/a_{cr}}$$

The procedure for applying figure 4 to determine the rotor-exit angle at the mean radius is as follows: With $V_{u,3}$ assigned at the mean radius, the work was calculated from equation (D2). The stagnation temperature and pressure at the rotor exit were then determined from

$$T'_3 = T'_1 - \frac{\text{work}}{c_p J}$$

and

$$p'_3 = p'_1 \left(1 - \frac{\text{work}}{c_p J \eta_T T'_1}\right)^{\frac{\gamma}{\gamma-1}}$$

Values of ρ'_3 and $a_{cr,3}$ were determined from the values of T'_3 and p'_3 thus obtained. When it is assumed that the specific weight flow at the mean radius is equal to the average specific weight flow, the corrected weight-flow parameter may be determined from the following expression:

$$\left(\frac{\rho V_x}{\rho' a_{cr}}\right)_3 = \frac{w}{A_3 \rho'_3 a_{cr,3}}$$

Then $\left(\frac{V_x}{a_{cr}}\right)_3$ is obtained from figure 4 and, when U_3 is known, the value of β_3 may be calculated.

2117

APPENDIX F

RADIAL VARIATION OF VELOCITY AT ROTOR ENTRANCE FOR RADIAL EQUILIBRIUM ACCOUNTING FOR STREAMLINE CURVATURE

The radial-equilibrium equation at a station midway between the stator exit and the rotor entrance, when constant entropy along the radius is assumed, may be written as (from reference 3, equation (14))

$$\frac{dh'}{dr} = \frac{V_u}{gr}\frac{d(V_u r)}{dr} + \frac{V_x}{g}\frac{dV_x}{dr} - \frac{V_x}{g}\frac{dV_r}{dx} \tag{F1}$$

When $\frac{dh'}{dr}$ is assumed equal to zero, equation (F1) may be written as

$$\frac{V_u^2}{r} - V_x\frac{dV_r}{dx} + V_u\frac{dV_u}{dr} + V_x\frac{dV_x}{dr} = 0 \tag{F2}$$

The radial component of velocity $V_r = V_x \tan\varphi$. (See fig. 1.) Differentiating V_r with respect to x and substituting the result in equation (F2) results in

$$\frac{V_u^2}{r} - V_x^2\frac{d(\tan\varphi)}{dx} - V_x\tan\varphi\frac{dV_x}{dx} + V_u\frac{dV_u}{dr} + V_x\frac{dV_x}{dr} = 0 \tag{F3}$$

It will be assumed that the maximum deflection of the streamlines occurs at this station. Therefore, φ equals zero and $\frac{d(\tan\varphi)}{dx} = \frac{d\varphi}{dx} = \frac{1}{C}$; equation (F3) may then be written as

$$\frac{V_u^2}{r} - \frac{V_x^2}{C} + V_u\frac{dV_u}{dr} + V_x\frac{dV_x}{dr} = 0 \tag{F4}$$

Nontwisted-rotor-blade turbines. - From vector-diagram considerations for nontwisted rotor blades,

$$\tan\beta = \frac{V_x}{V_u - U} = \text{constant}$$

or

$$V_u = V_x\cot\beta + U \tag{F5}$$

2117

Differentiation with respect to the radius gives

$$\frac{dV_u}{dr} = \cot \beta \frac{dV_x}{dr} + \omega \tag{F6}$$

Substituting equations (F5) and (F6) in equation (F4) and simplifying result in the following expression for $\frac{dV_x}{dr}$:

$$\frac{dV_x}{dr} = - \frac{\frac{(V_x \cot \beta + U)^2}{r} - \frac{V_x^{\ 2}}{C} + \omega (V_x \cot \beta + U)}{V_x + V_x \cot^2 \beta + U \cot \beta} \tag{F7}$$

Using the identity

$$\frac{dV_x}{dr} \equiv U \frac{d\left(\frac{V_x}{U}\right)}{dr} + \frac{V_x}{U} \frac{dU}{dr}$$

multiplying equation (F7) by r_m/U and the numerator and the denominator of the right member by $1/U$, and simplifying yield

$$\frac{d\left(\frac{V_x}{U}\right)}{d\left(\frac{r}{r_m}\right)} = - \frac{1}{\frac{r}{r_m}} \frac{2 + 4\left(\frac{V_x}{U}\right) \cot \beta + \left(\frac{V_x}{U}\right)^2 \left[- \frac{r_m}{C} \left(\frac{r}{r_m}\right) + (1 + 2 \cot^2 \beta)\right]}{\frac{V_x}{U} \csc^2 \beta + \cot \beta} \tag{4}$$

<u>Free-vortex turbines.</u> - For free-vortex flow,

$$V_u r = \text{constant}$$

Differentiating with respect to r and multiplying by $\frac{V_u}{r}$ yield

$$V_u \frac{dV_u}{dr} + \frac{V_u^{\ 2}}{r} = 0 \tag{F9}$$

Substituting equation (F9) in equation (F4) and simplifying result in

$$\frac{dV_x}{dr} = \frac{V_x}{C} \tag{5}$$

REFERENCES

1. Ellerbrock, Herman H., Jr.: N.A.C.A. Investigations of Gas-Turbine-Blade Cooling. Jour. Aero. Sci., vol. 15, no. 12, Dec. 1948, pp. 721-730.

2. Eckert, and Korbacher: The Flow through Axial Turbine Stages of Large Radial Blade Length. NACA TM 1118, 1947.

3. Wu, Chung-Hua, and Wolfenstein, Lincoln: Application of Radial-Equilibrium Condition to Axial-Flow Compressor and Turbine Design. NACA Rep. 955, 1950. (Formerly TN 1795, 1950.)

4. Willers, Fr. A.: Practical Analysis. Dover Pub., Inc., 1948, pp. 375-386.

2117

2117

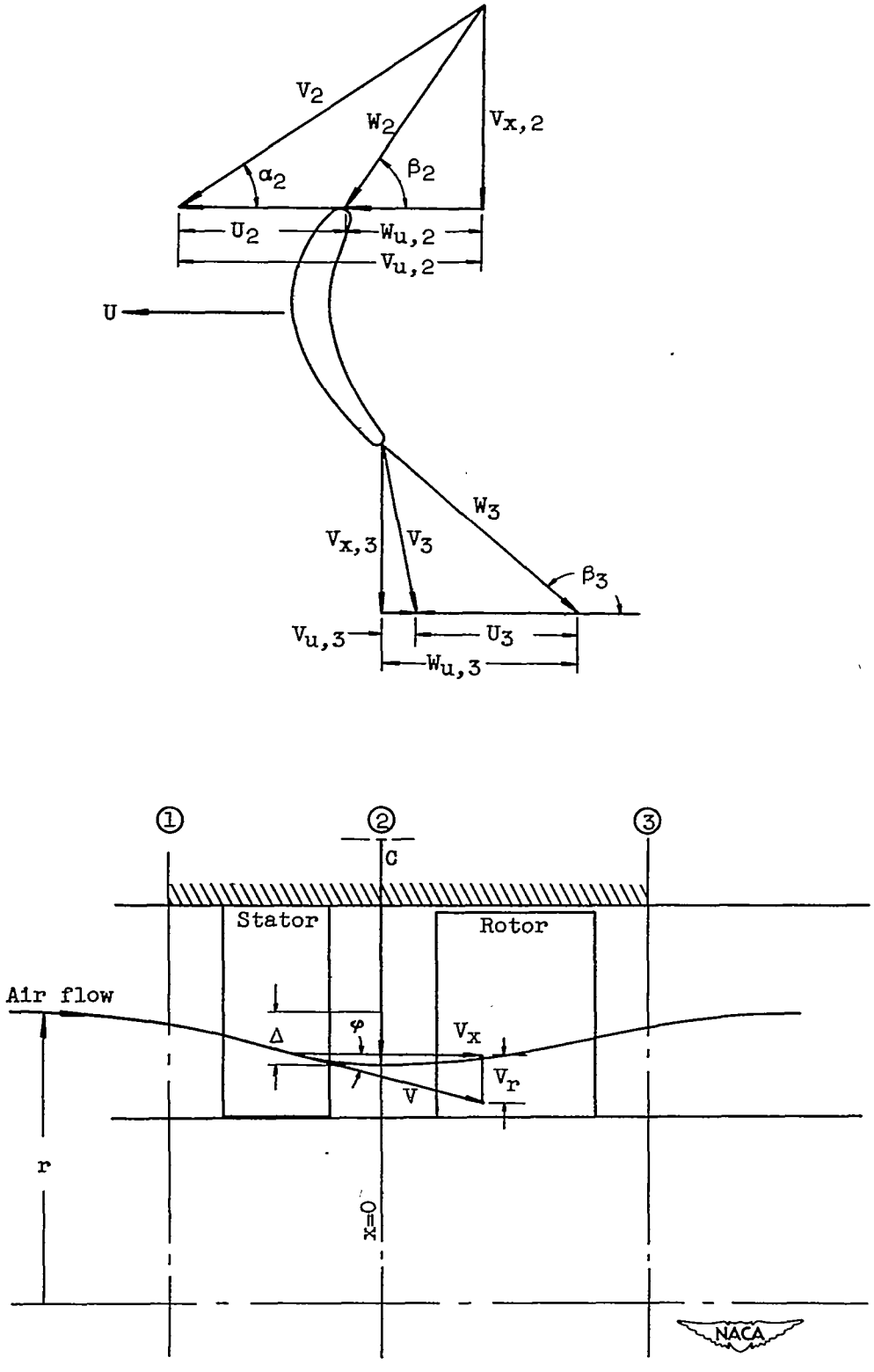

Figure 1. - Velocity vector diagram and section of turbine through axial-radial plane.

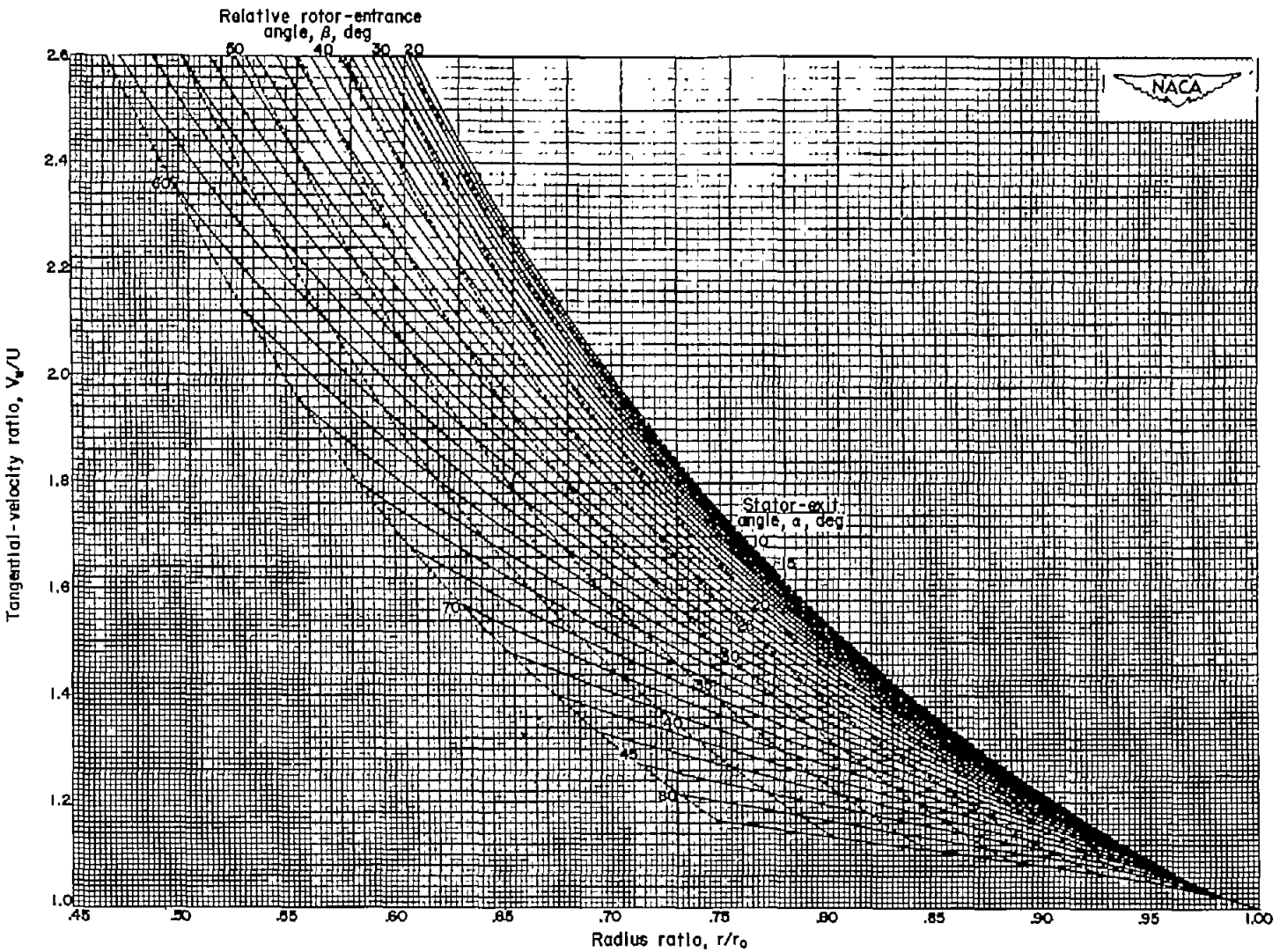

Figure 2. - Variation of tangential-velocity ratio with radius ratio for constant rotor-entrance angles. (A 17- by 22-in. print of this fig. is attached.)

2117

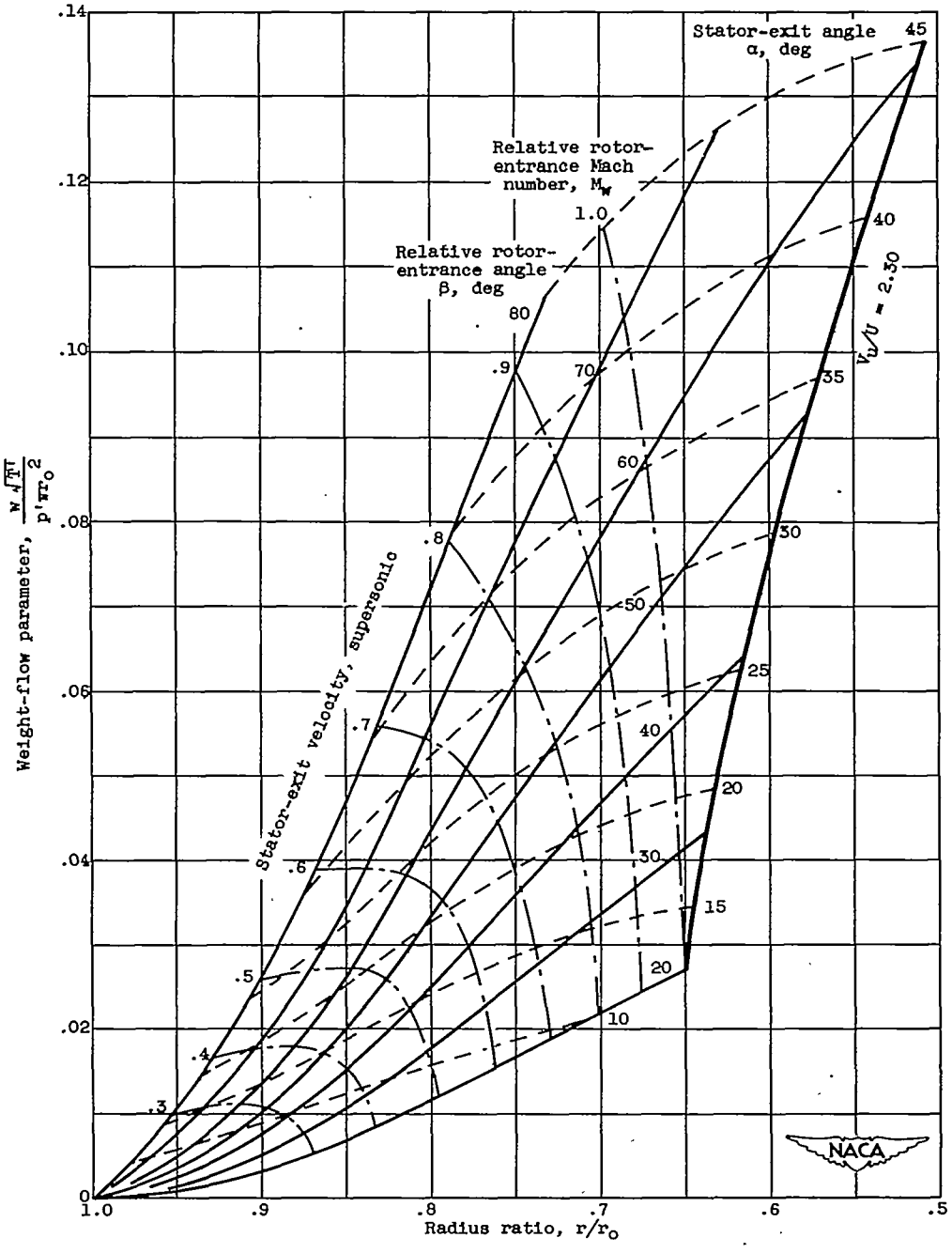

(a) $M_o = 1.0$.

Figure 3. - Variation of weight-flow parameter, stator-exit angle, and relative rotor-entrance Mach number with radius ratio for constant relative rotor-entrance angle ($\gamma = 1.3$).

2117

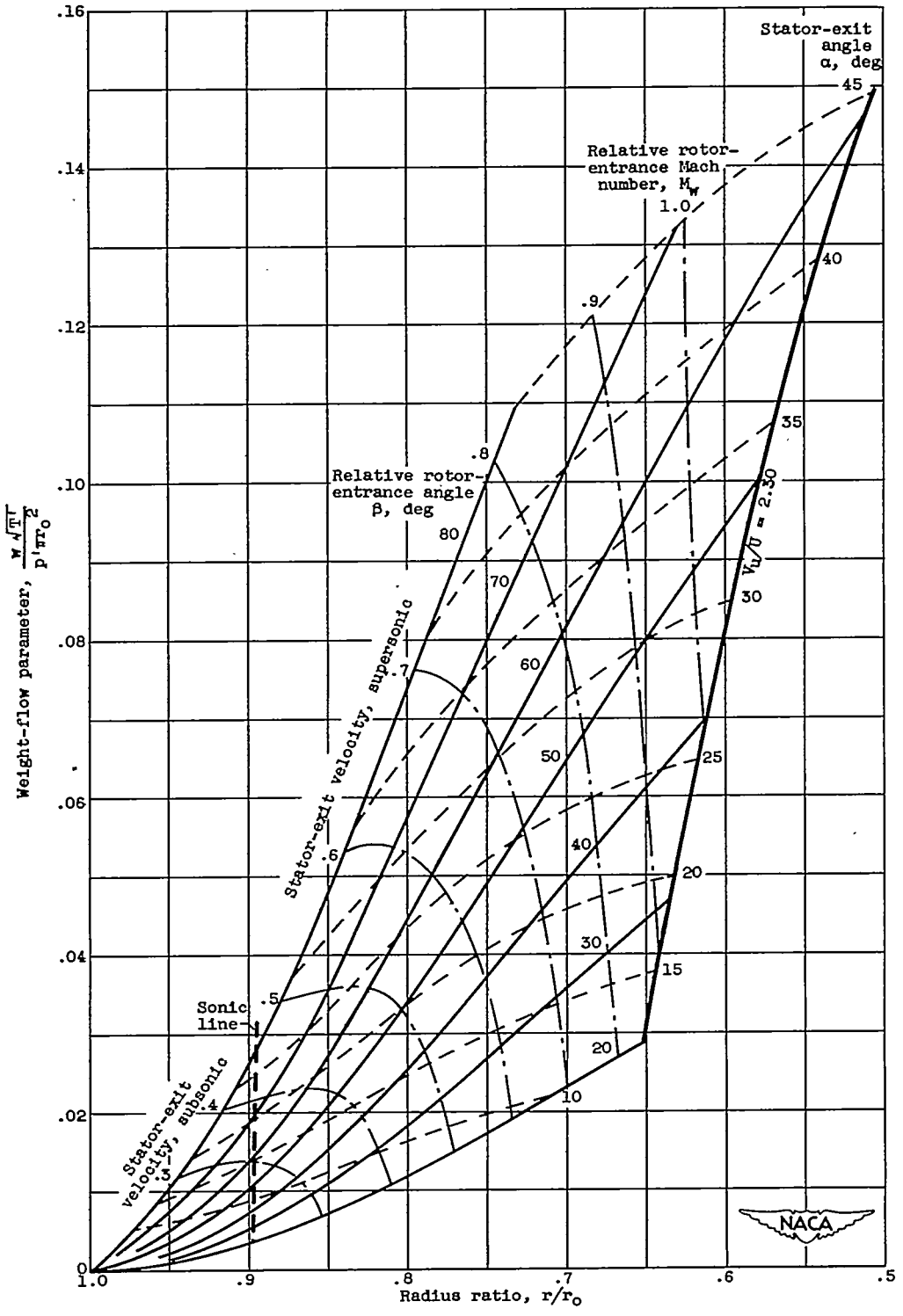

(b) $M_o = 0.9$.

Figure 3. - Continued. Variation of weight-flow parameter, stator-exit angle, and relative rotor-entrance Mach number with radius ratio for constant relative rotor-entrance angle ($\gamma = 1.3$).

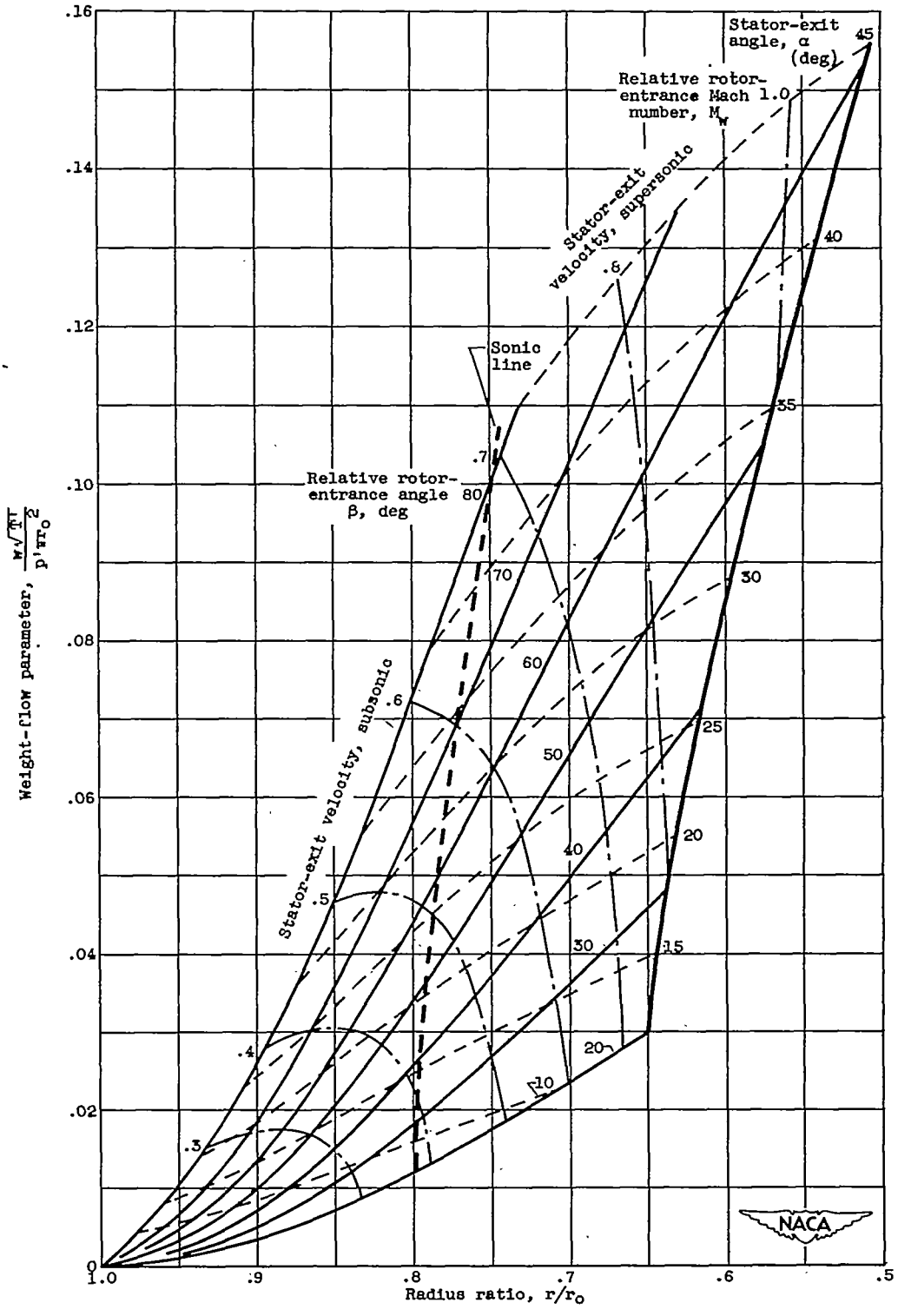

(c) $M_o = 0.8$.

Figure 3. - Continued. Variation of weight-flow parameter, stator-exit angle, and relative rotor-entrance Mach number with radius ratio for constant relative rotor-entrance angle ($\gamma = 1.3$).

2117

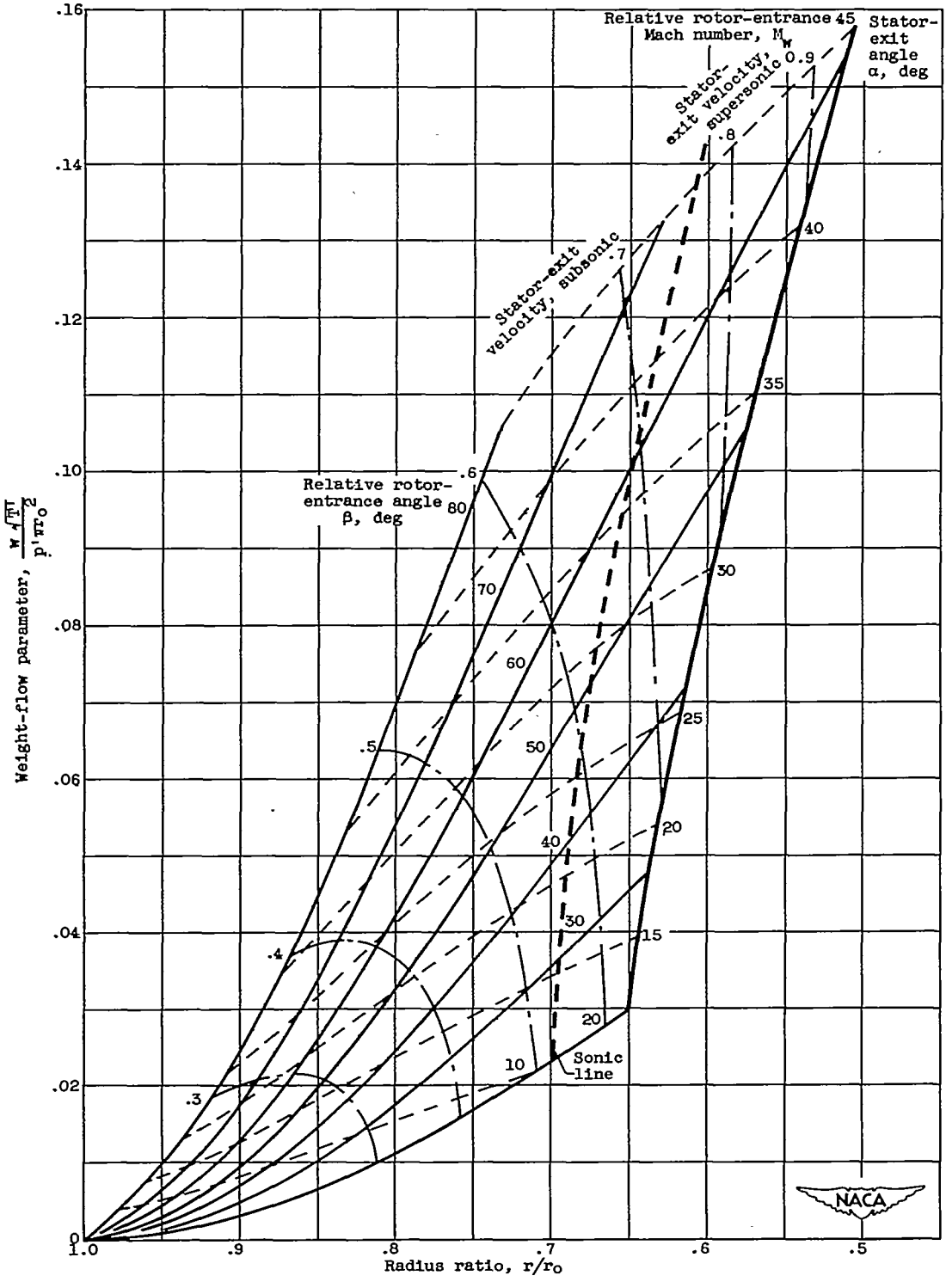

(d) $M_o = 0.7$.

Figure 3. - Continued. Variation of weight-flow parameter, stator-exit angle, and relative rotor-entrance Mach number with radius ratio for constant relative rotor-entrance angle ($\gamma = 1.3$).

2117

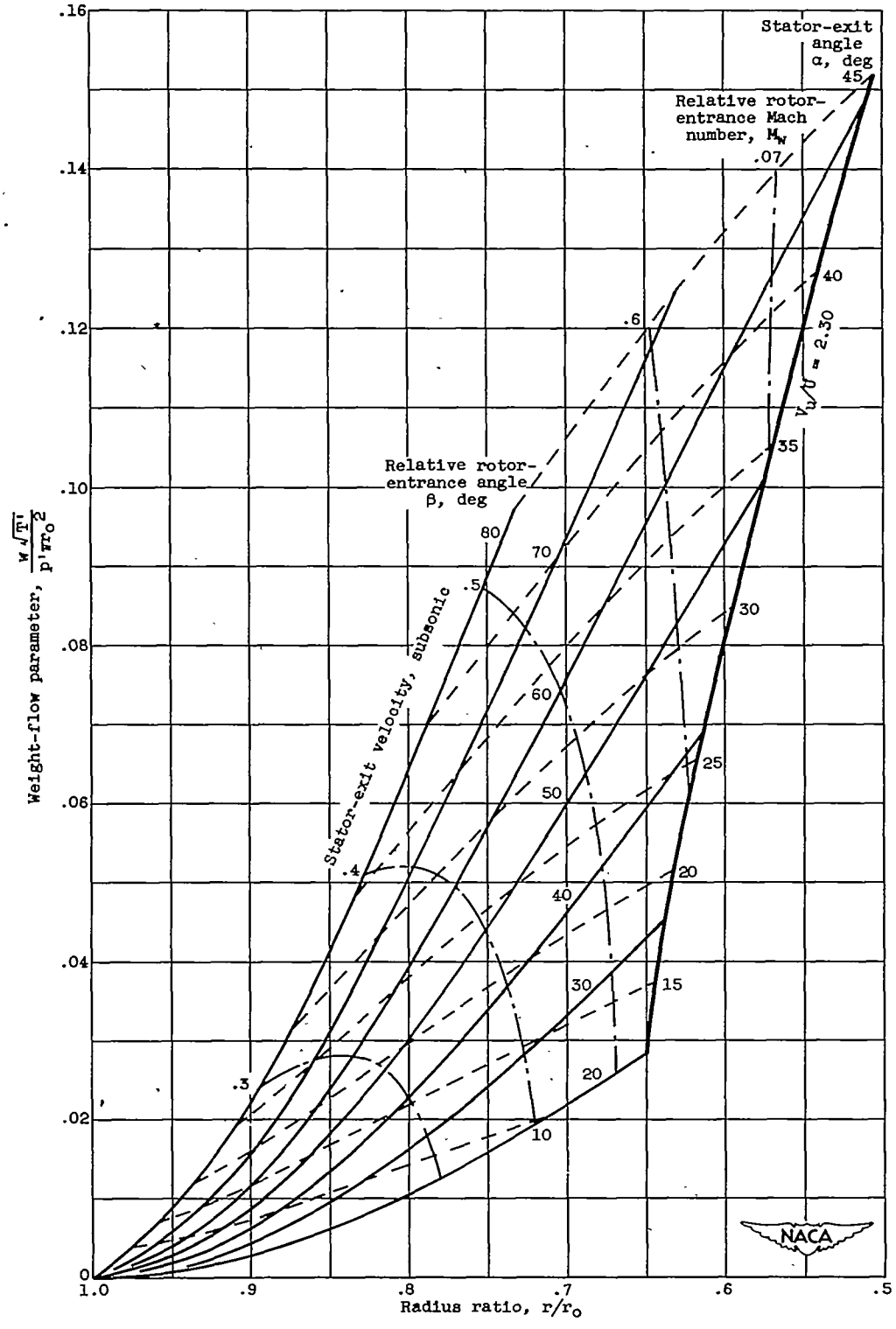

(e) $M_o = 0.6$.

Figure 3. - Continued. Variation of weight-flow parameter, stator-exit angle, and relative rotor-entrance Mach number with radius ratio for constant relative rotor-entrance angle ($\gamma = 1.3$).

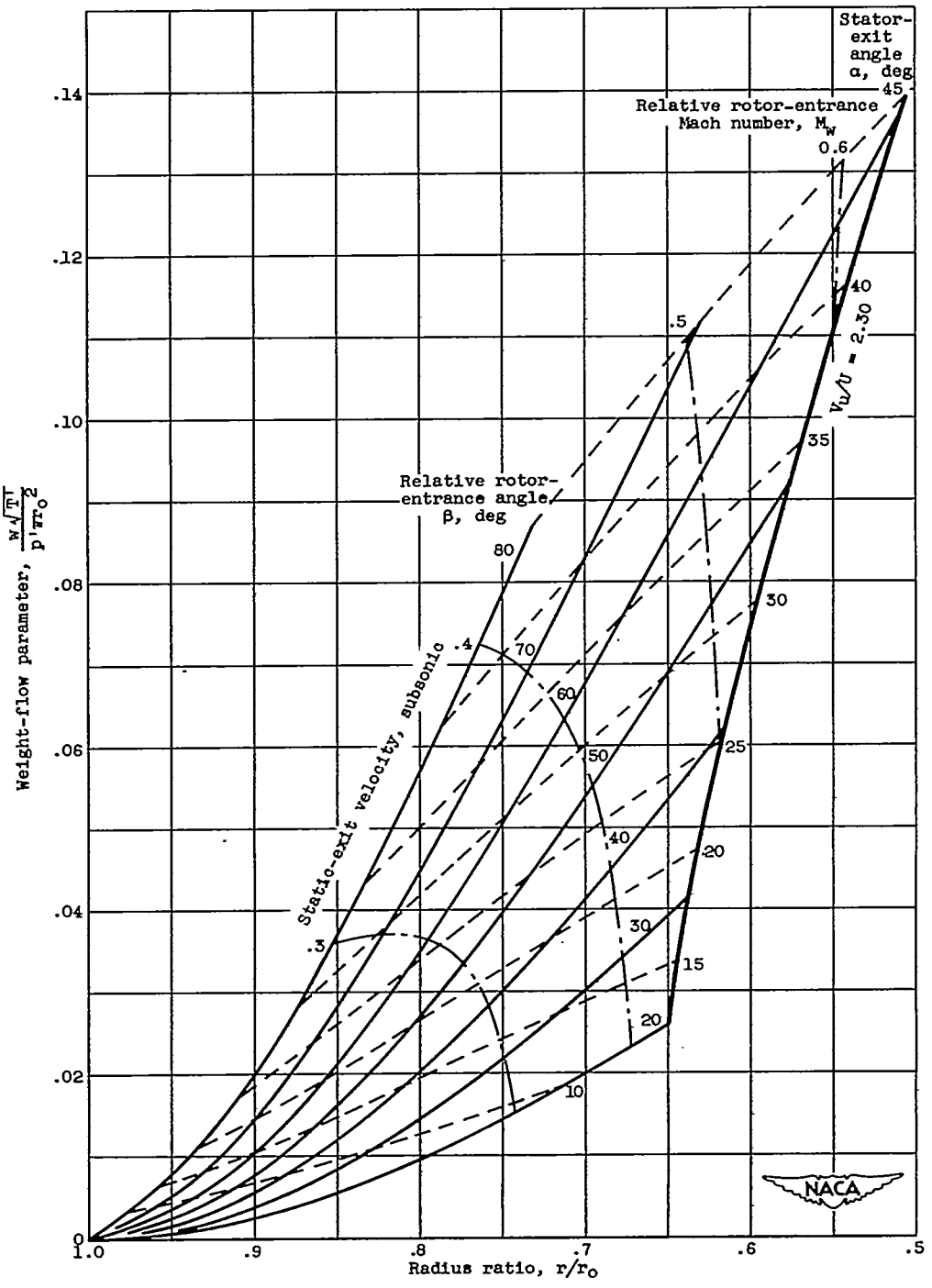

(f) M_o = 0.5.

Figure 3. - Concluded. Variation of weight-flow parameter, stator-exit angle, and relative rotor-entrance Mach number with radius ratio for constant relative rotor-entrance angle (γ = 1.3).

2117

2117

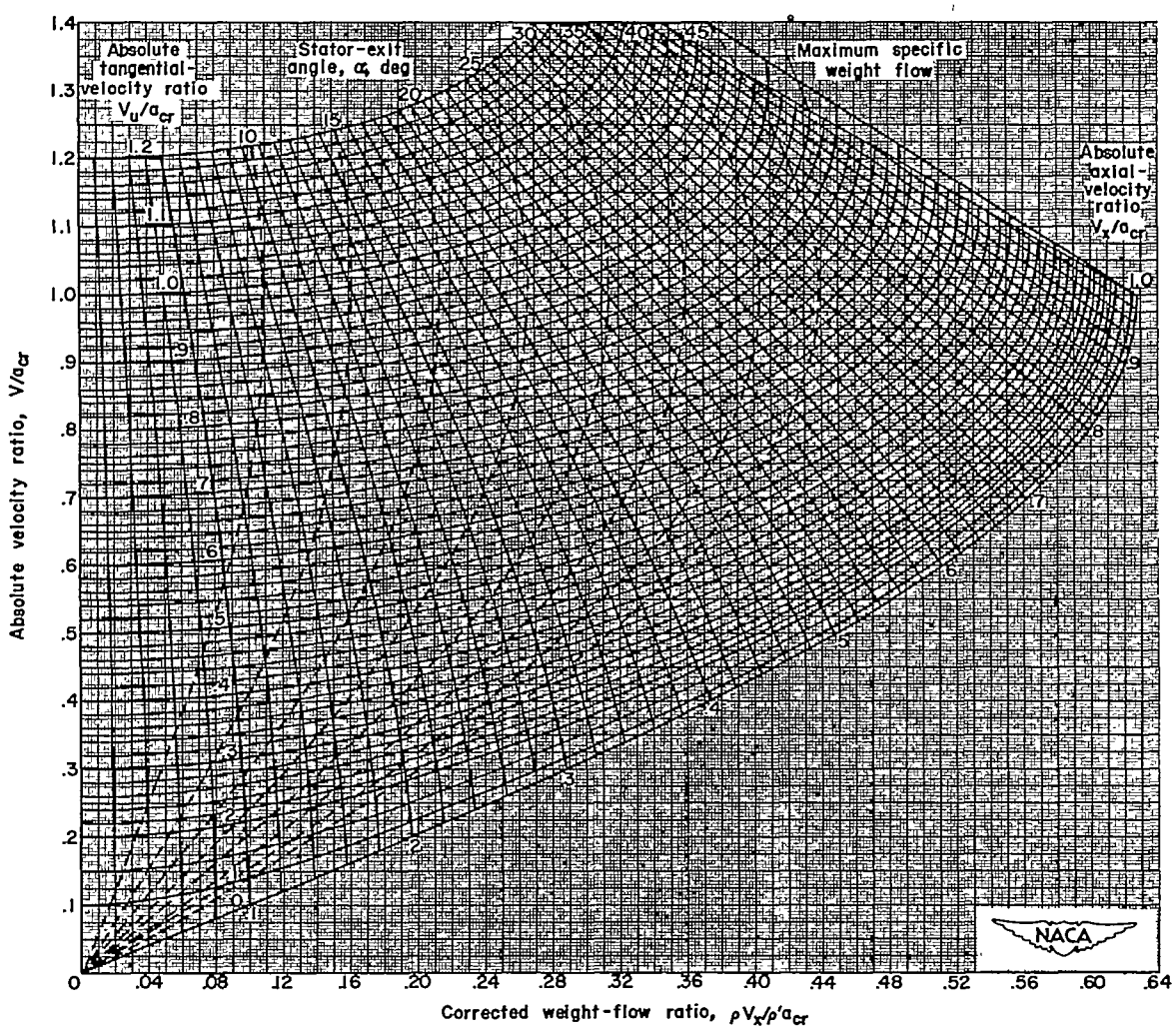

Figure 4. - Variation of absolute velocity ratio with corrected weight-flow ratio for constant absolute tangential-velocity ratio and absolute axial-velocity ratio (γ = 1.3). (A 17- by 22-in. print of this fig. is attached.)

2117

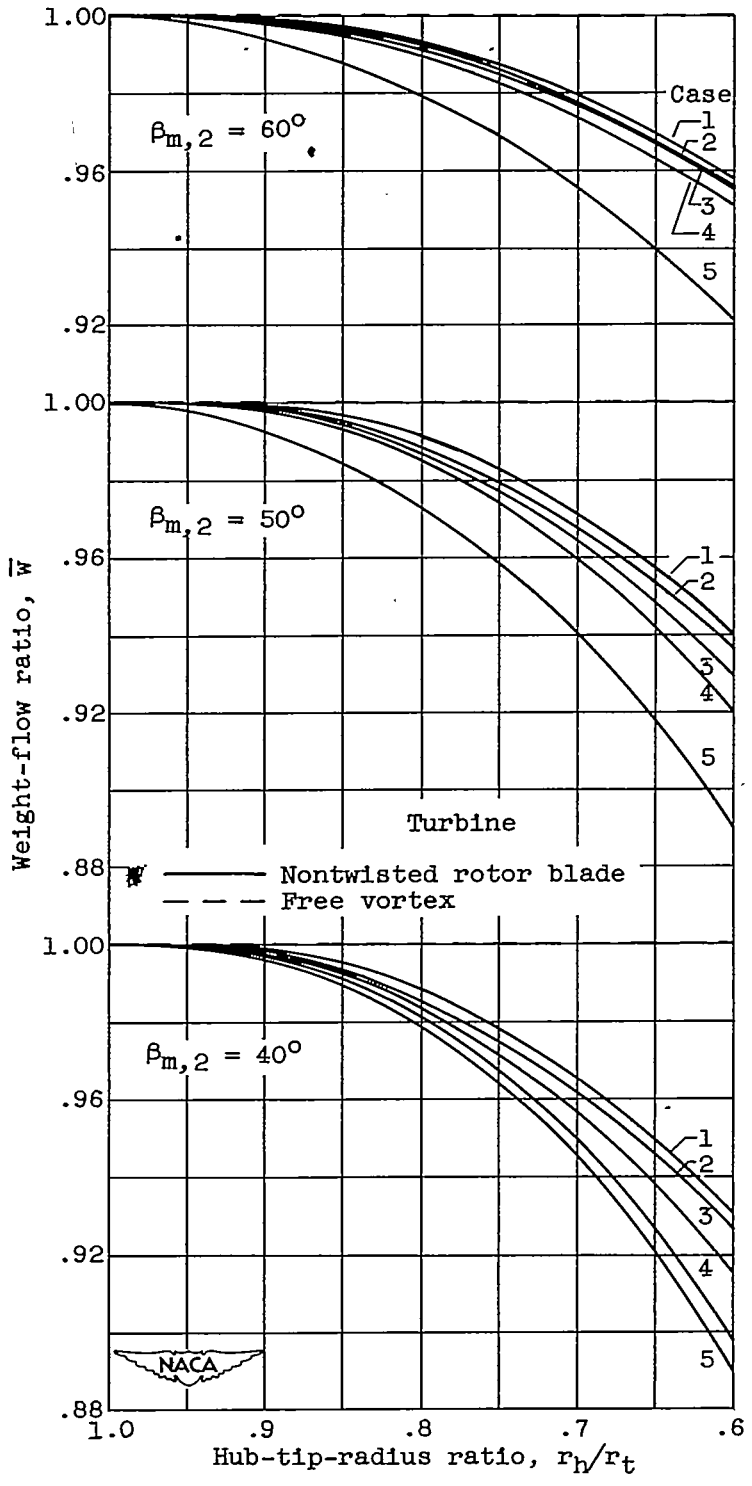

Figure 5. - Variation of weight-flow ratio with hub-tip-radius ratio for nontwisted-rotor-blade and free-vortex turbines for same mean-radius conditions.

2117

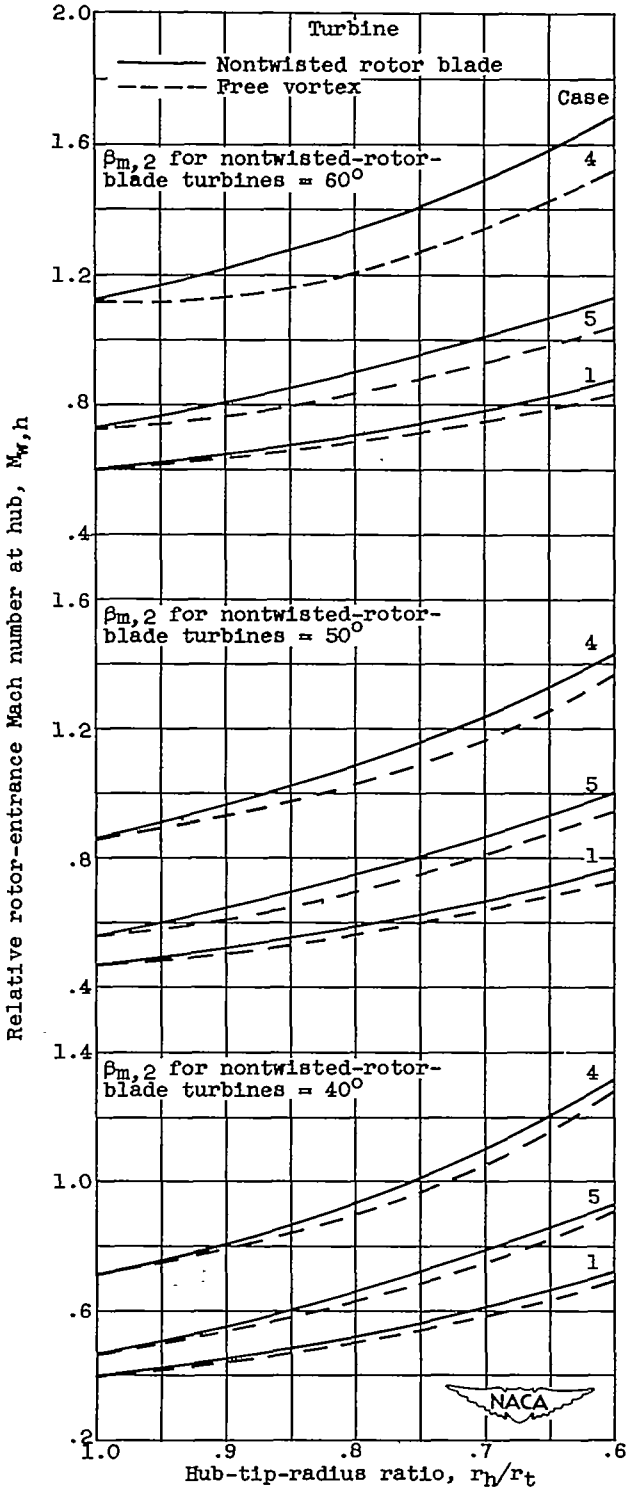

Figure 6. - Variation of hub relative rotor-entrance Mach number with hub-tip-radius ratio for nontwisted-rotor-blade and free-vortex turbines for equal weight flow per unit annulus area.

2117

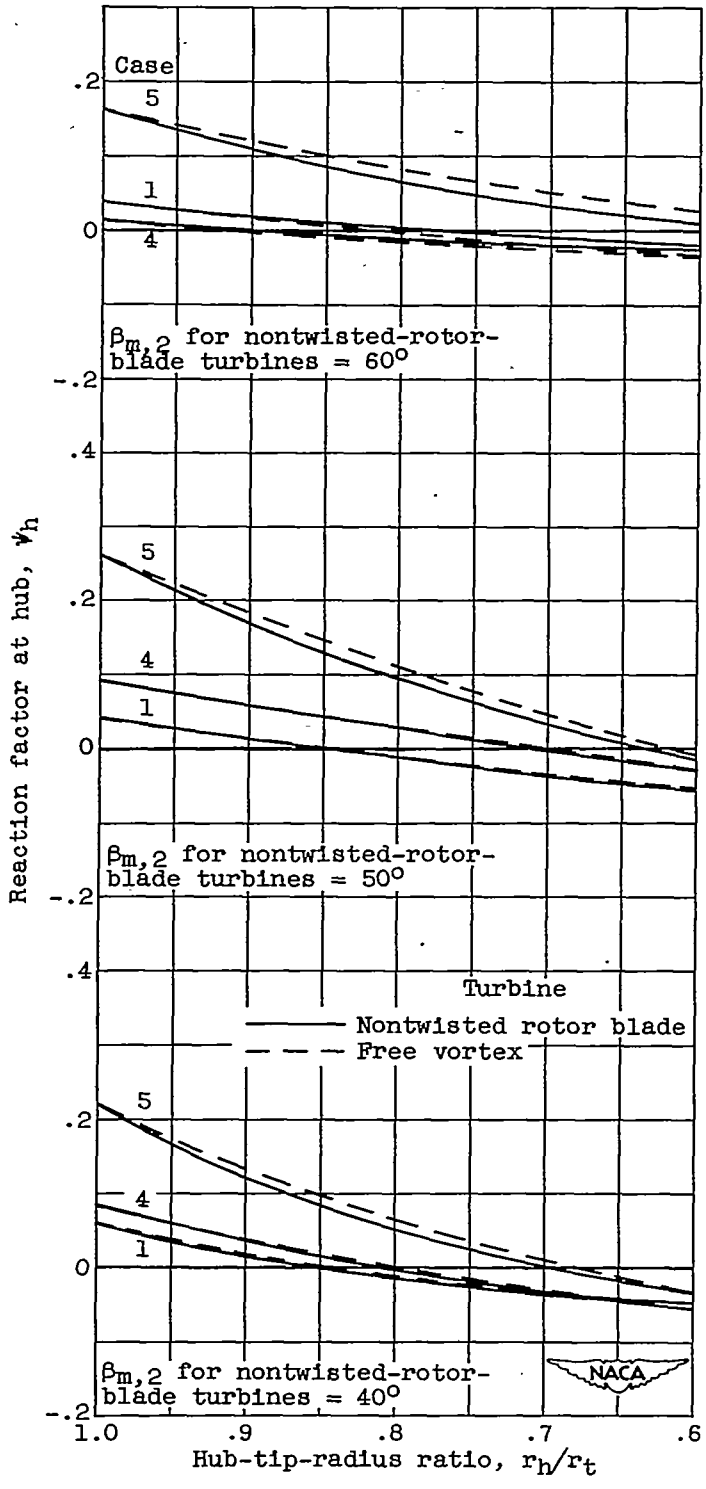

Figure 7. - Variation of hub reaction factor with hub-tip-radius ratio for nontwisted-rotor-blade and free-vortex turbines for equal weight flow per unit annulus area.

2117

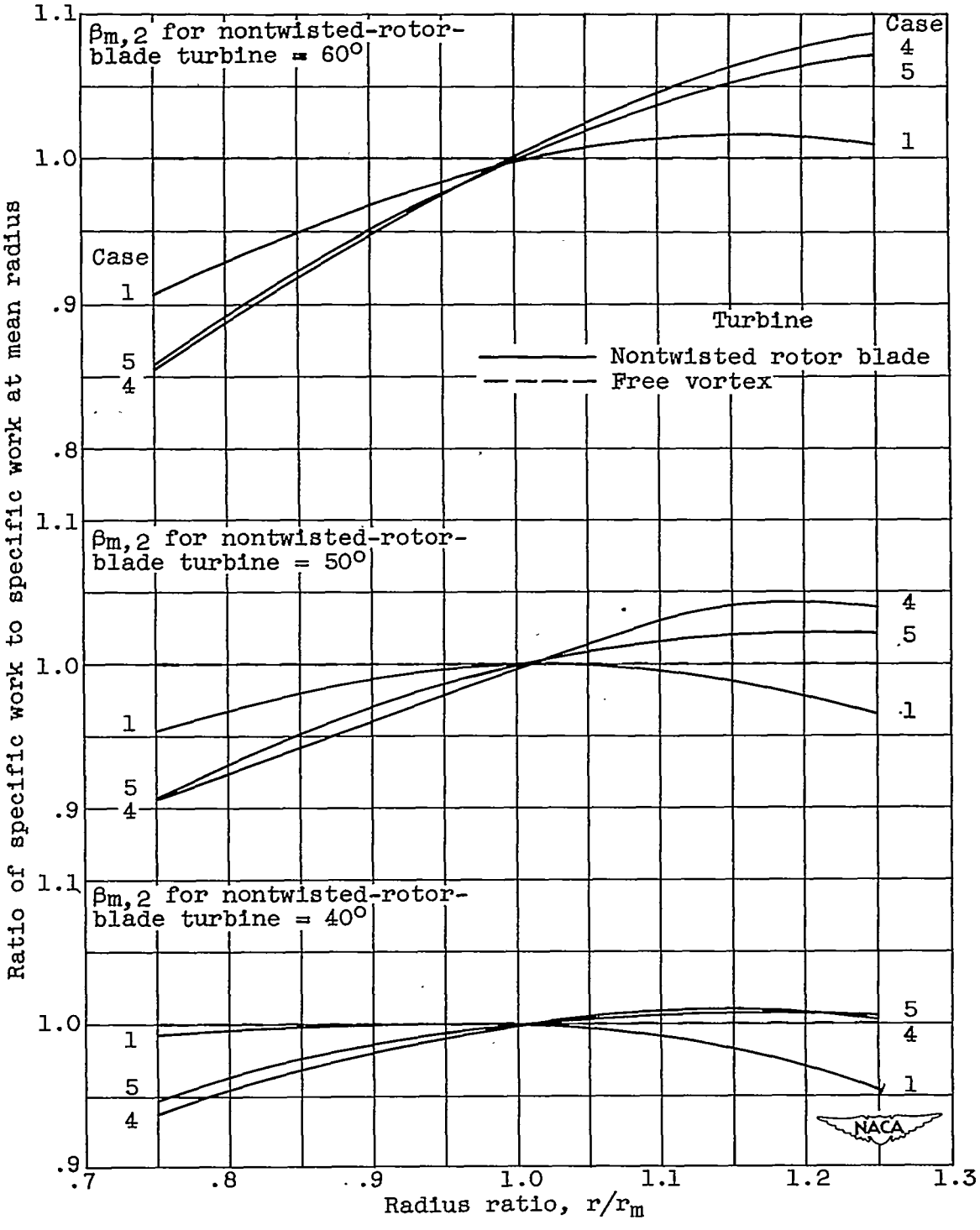

Figure 8. - Variation of ratio of specific work to specific work at mean radius with radius ratio for nontwisted rotor-blade and free-vortex turbines.

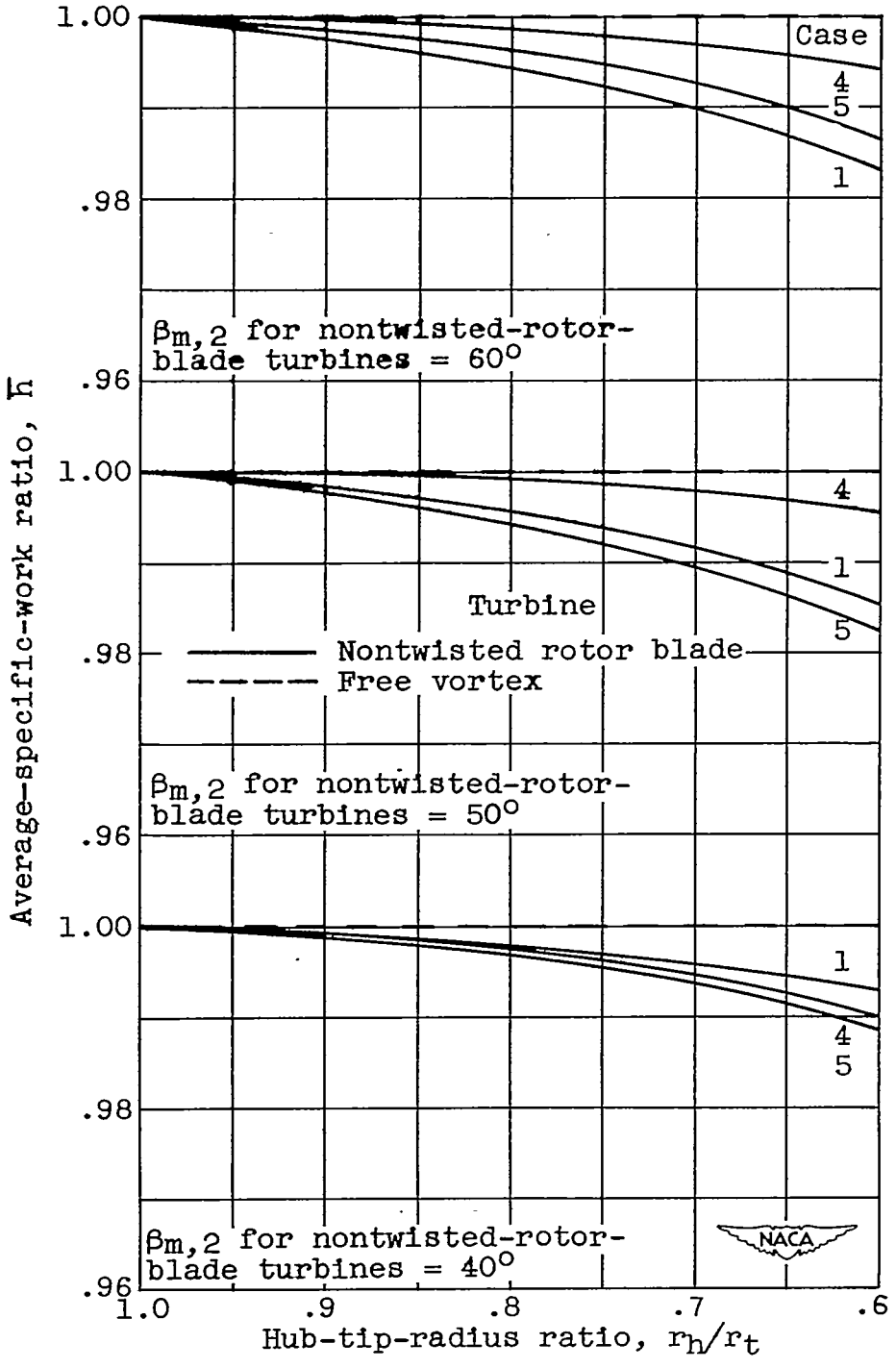

Figure 9. - Variation of average-specific-work ratio with hub-tip-radius ratio for nontwisted-rotor-blade and free-vortex turbines for equal weight flow per unit annulus area.

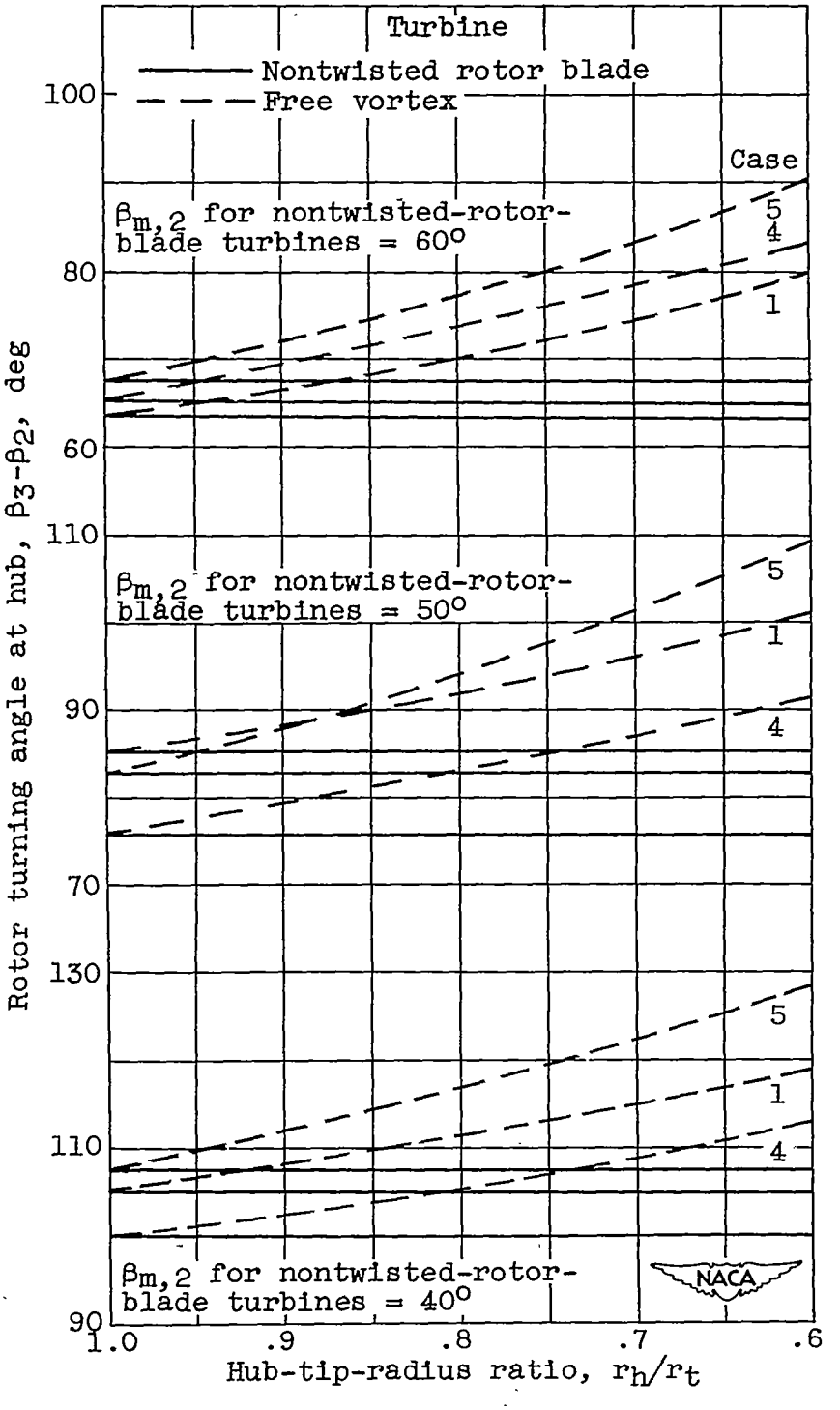

Figure 10. - Variation of rotor-hub turning angle with hub-tip-radius ratio for nontwisted-rotor-blade and free-vortex turbines for equal weight flow per unit annulus area.

2117

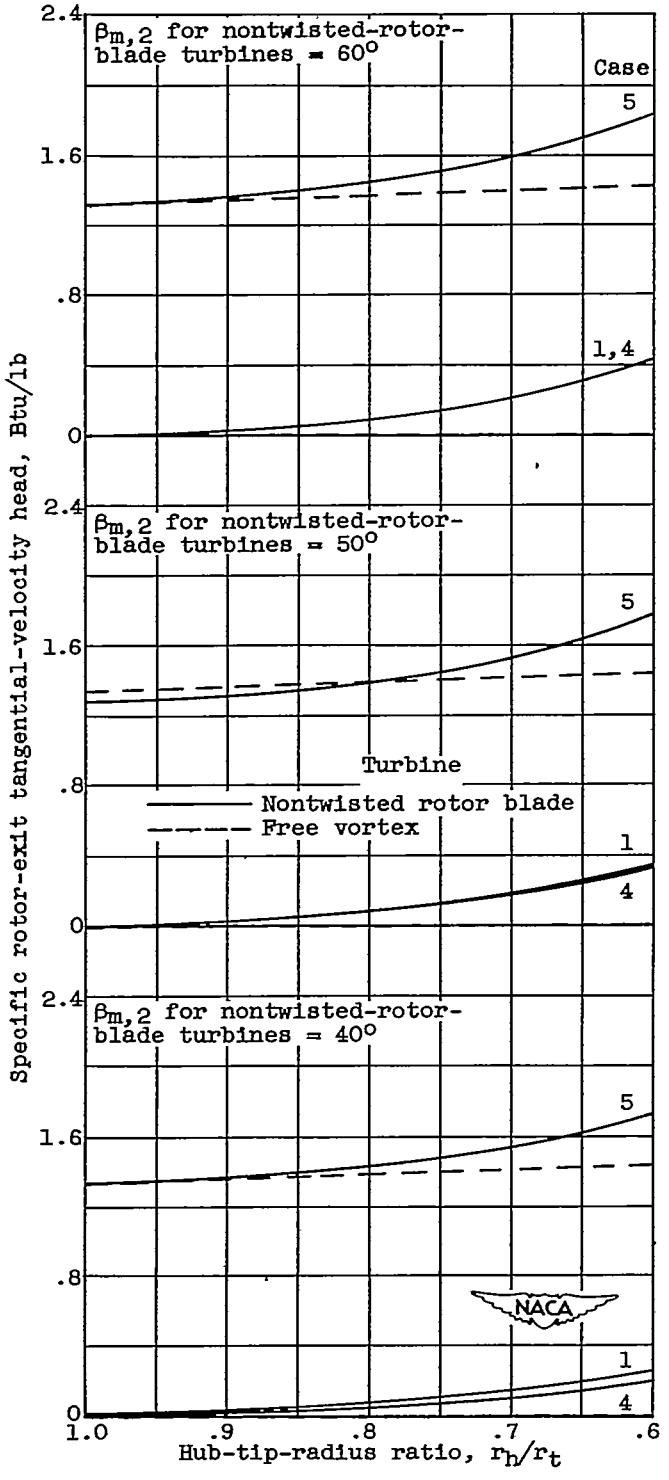

Figure 11. - Variation of specific rotor-exit tangential-velocity head with hub-tip-radius ratio for nontwisted-rotor-blade and free-vortex turbines for equal weight flow per unit annulus area.

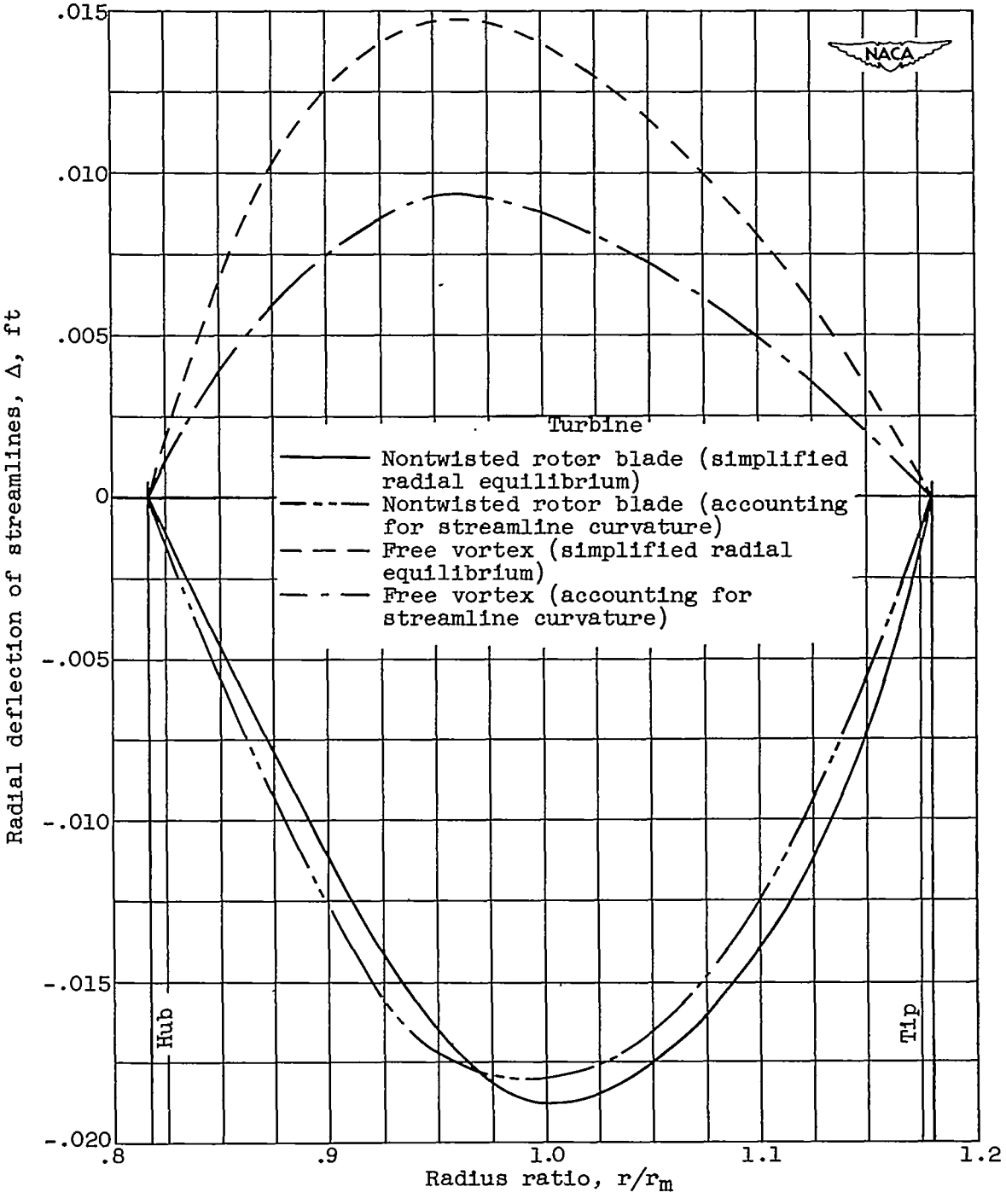

Figure 12. - Variation of radial deflection of streamlines midway between rotor and stator with radius ratio for typical turbine example.

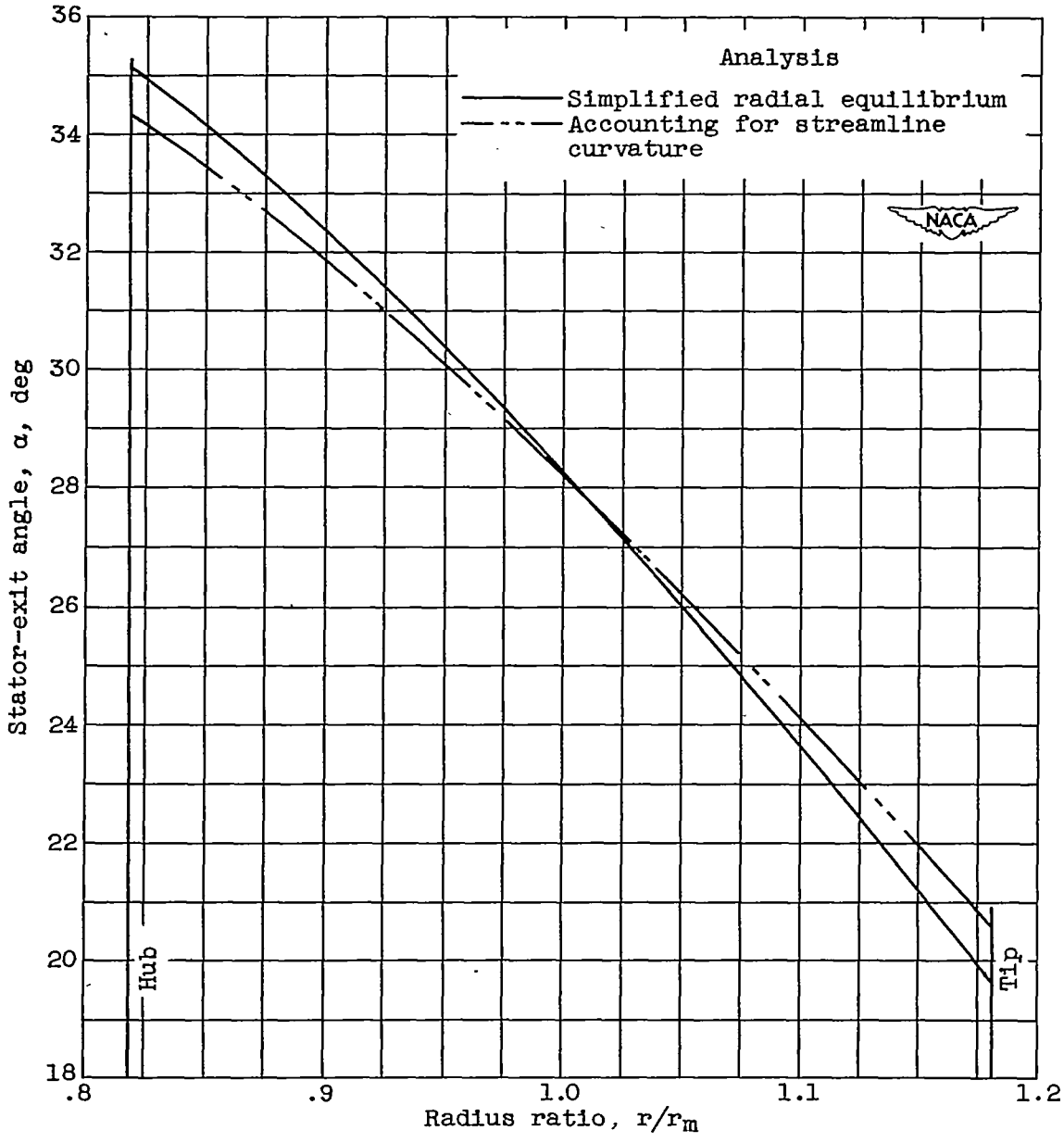

Figure 13. - Variation of stator-exit angle with radius ratio for typical example of nontwisted-rotor-blade turbine.

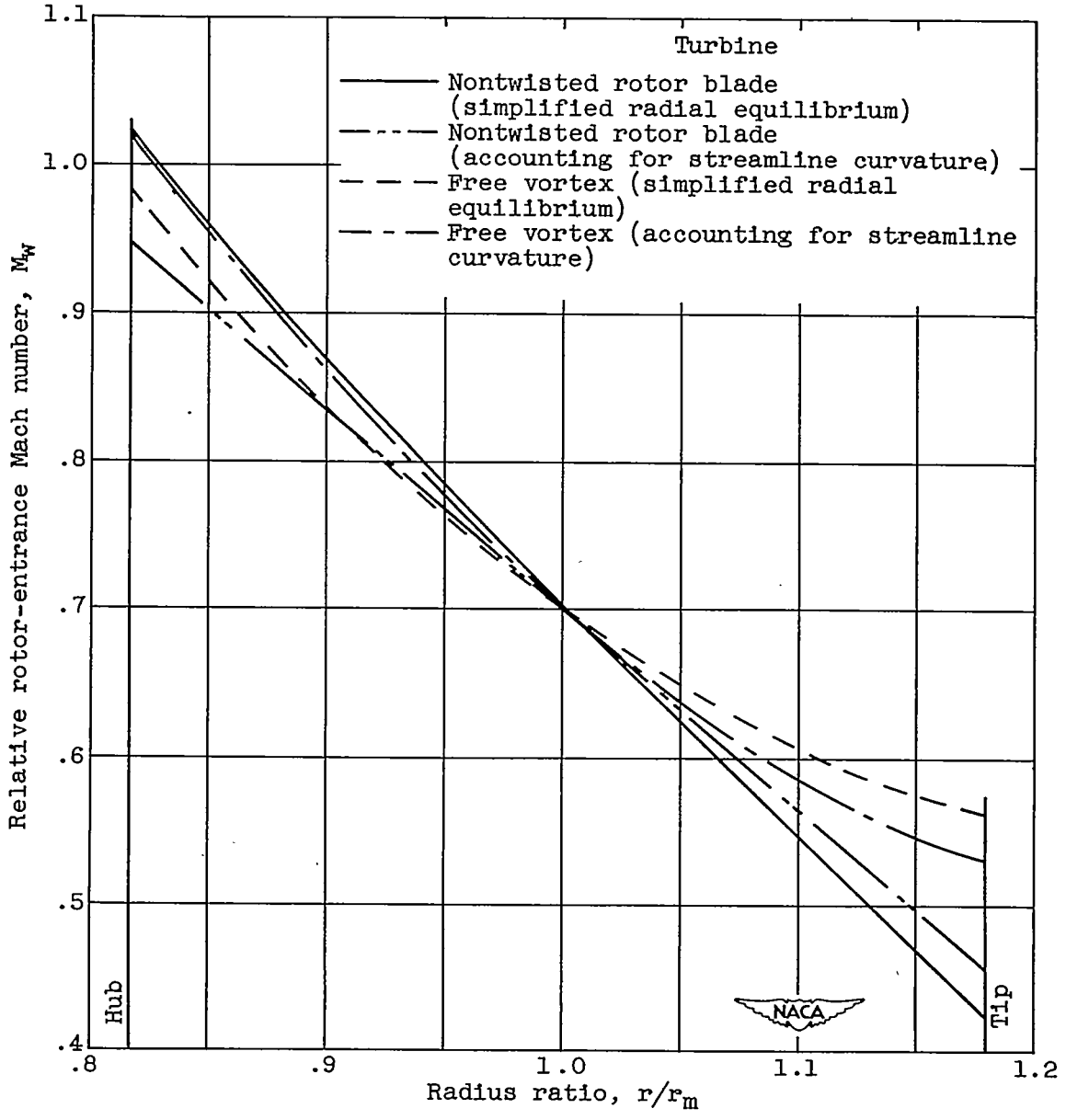

Figure 14. - Variation of relative rotor-entrance Mach number with radius ratio for typical turbine examples.

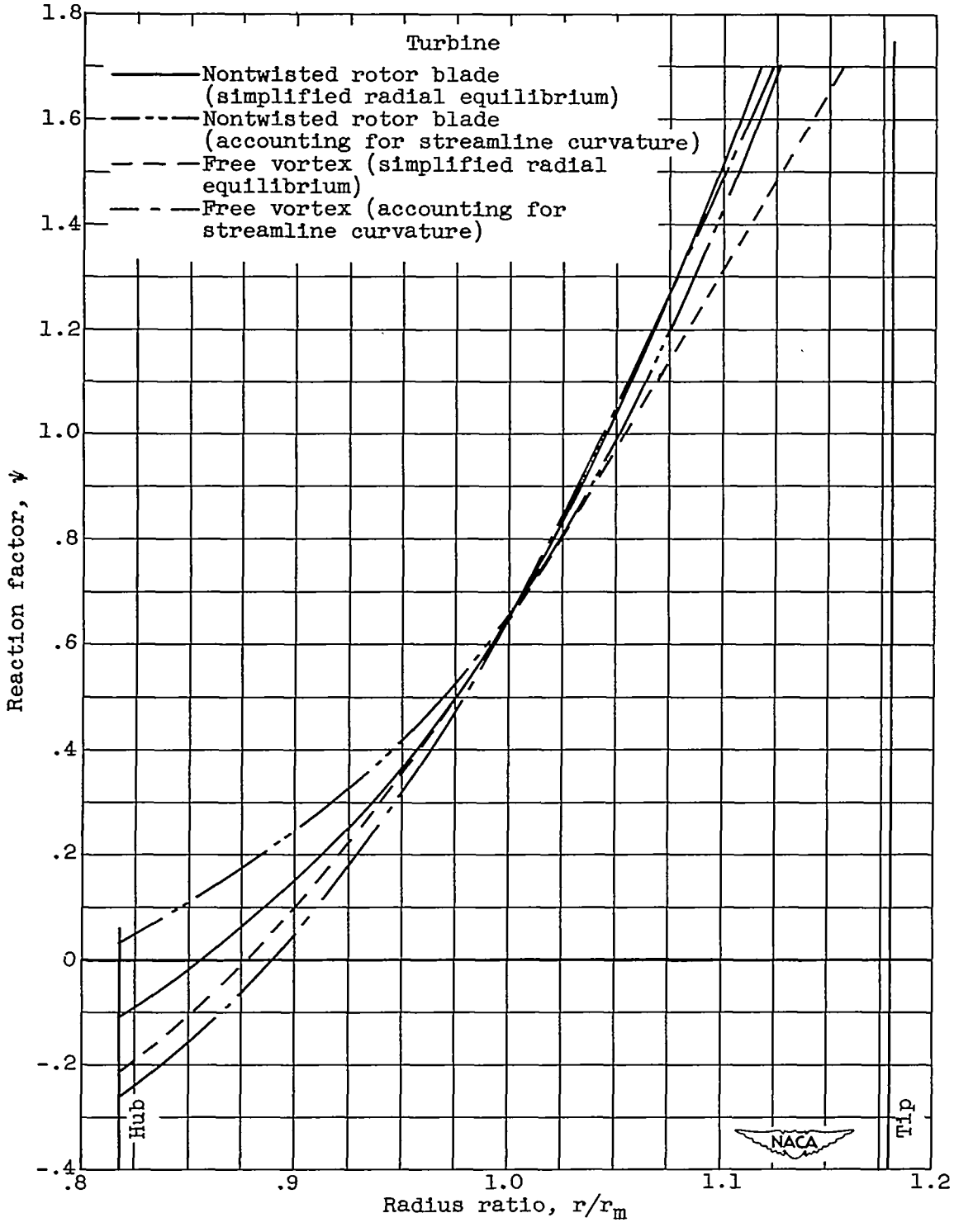

Figure 15. - Variation of reaction factor with radius ratio for typical turbine example.